NEUROSCIENCE

# Cholinergic signaling to CA1 astrocytes controls fear extinction

**Yulan Li[1]†, Lixuan Li[2]†, Yibei Wang[1,3]†, Xinyi Li[1], Xiaopeng Ding[1], Lingjie Li[1], Fan Fei[1], Yanrong Zheng[1], Li Cheng[1], Shumin Duan[2], Vladimir Parpura[3], Yi Wang[1,2]*, Zhong Chen[1,2]***



**Fear extinction is an evolutionarily conserved biological process that allows an organism to better re-adapt; its deficits can lead to psychiatric disorders. Fear extinction is considered to rely mostly on neuronal function. However, whether and how astrocytes contribute to fear extinction is largely unknown. Here, we show that hippocampal CA1 astrocytes exhibit de novo $Ca^{2+}$ dynamics during fear extinction. Inhibition of these astrocytic $Ca^{2+}$ dynamics impairs, while their activation facilitates, fear extinction. In this regulation of fear extinction, the posterior basal forebrain (pBF) cholinergic input to hippocampus drives CA1 astrocytic $Ca^{2+}$ dynamics through the activation of α4 and α7 subunits of nicotinic acetylcholine receptors. Clinically used acetylcholinesterase inhibitor donepezil increases CA1 astrocytic $Ca^{2+}$ dynamics and facilitates fear extinction. Thus, our findings demonstrate a previously unrecognized and crucial pathway from pBF cholinergic neurons to CA1 astrocytes that governs natural fear extinction. This neuron-glia signaling pathway may constitute a promising target for treatment of fear- and anxiety-related disorders.**

## INTRODUCTION

Fear extinction refers to a critical biological process in which learned fear memory, associated with an aversive stimulus, diminishes through a prolonged or repeated exposure to previous fear contexts or cues in the absence of an aversive stimulus. This fundamental process is essential for re-adaptation and survival, and its deficits can lead to various psychiatric disorders, such as post-traumatic stress disorder (PTSD) and anxiety disorder (*1*, *2*). Exposure-based therapy is currently the most commonly available clinical treatment for fear- and anxiety-related disorders (*3*–*6*). However, the efficacy of an exposure-based therapy remains limited, which places a strong emphasis on identifying other key contributors to fear extinction to improve treatments of fear- and anxiety-related disorders (*7*).

Previous studies have highlighted morphofunctional alterations of neural circuits in brain regions associated with fear extinction, e.g., in the amygdala, hippocampus, and medial prefrontal cortex (mPFC) (i.e., the limbic system) (*8*–*10*). These alterations are accompanied with the regulation of neuronal activity, synaptic plasticity, and network oscillations during extinction (*11*–*16*). Astrocytes are considered as active partners in synaptic processing via the tripartite synapse (*17*). They respond to synaptic activity with changes in cytosolic $Ca^{2+}$ concentration, the output of which, i.e., gliotransmission, can in turn affect synaptic, circuit activity and associated behavioral outputs (*18*–*21*). Thus, these glial cells play an important role in various physiological or pathological processes. We and others showed that manipulation of astrocyte activity affects fear memory (*19*, *22*–*24*). However, whether and how astrocytes are involved in, and contribute to, fear extinction remains unknown. Moreover, apart from the classic role of excitatory and inhibitory neural circuits in extinction being the focus of much research, the role of neuromodulation emerges in this process (*25*). Neuromodulators have been found to mediate $Ca^{2+}$ activity in astrocytes (*26*, *27*), and among various neuromodulators, acetylcholine (ACh) is considered crucial in learning and memory (*28*, *29*). Consequently, we addressed a thus far unsolicited question of whether astrocyte activity and ACh signaling are coupled and contribute to the regulation of fear extinction.

Here, we investigated the role of hippocampal astrocytes and the mechanism by which they govern fear extinction. We discovered aversive experience–primed and context-dependent astrocytic $Ca^{2+}$ responses in the hippocampal CA1 region; these astrocytic $Ca^{2+}$ dynamics are sufficient and necessary for governing fear extinction. We further revealed that a crucial neuron-glia signaling pathway [i.e., the posterior basal forebrain (pBF) cholinergic input to CA1 astrocytes] fundamentally contributes to the control of natural fear extinction. Moreover, the clinically relevant acetylcholinesterase inhibitor donepezil increased astrocytic $Ca^{2+}$ activity and enhanced fear extinction. These findings suggest that the pBF cholinergic input to CA1 astrocytes is a promising therapeutic target for fear- and anxiety-related disorders.

## RESULTS

### De novo responses of CA1 astrocytes during contextual fear extinction

To explore whether astrocytes are engaged in fear extinction, we used a contextual fear extinction paradigm (Fig. 1, A to C, and fig. S1A). On day 1, the extinction group received contextual fear conditioning (CFC) in which four rounds of electric foot shocks served as unconditioned stimulus (US). On day 2, mice were returned to the conditioning box for 40 min in the absence of foot shocks for contextual fear extinction training. On day 3, the mice were tested for the 5-min extinction memory retrieval in the conditioning box (Fig. 1C, top). The non-extinction group went through the same protocol as the extinction group on days 1 and 3, but remained in their home

[1]Zhejiang Key Laboratory of Neuropsychopharmacology, School of Pharmaceutical Science, and Department of Physiology, School of Basic Medical Science, Zhejiang Chinese Medical University, Hangzhou 310053, China. [2]Department of Neurology, Second Affiliated Hospital, School of Medicine, Zhejiang University, Hangzhou, Zhejiang 310009, China. [3]International Translational Neuroscience Research Institute, School of Pharmaceutical Science, School of Basic Medical Science, Zhejiang Chinese Medical University, Hangzhou 310053, China.
*Corresponding author. Email: wang-yi@zju.edu.cn (Y.W.); chenzhong@zju.edu.cn (Z.C.)
†These authors contributed equally to this work.

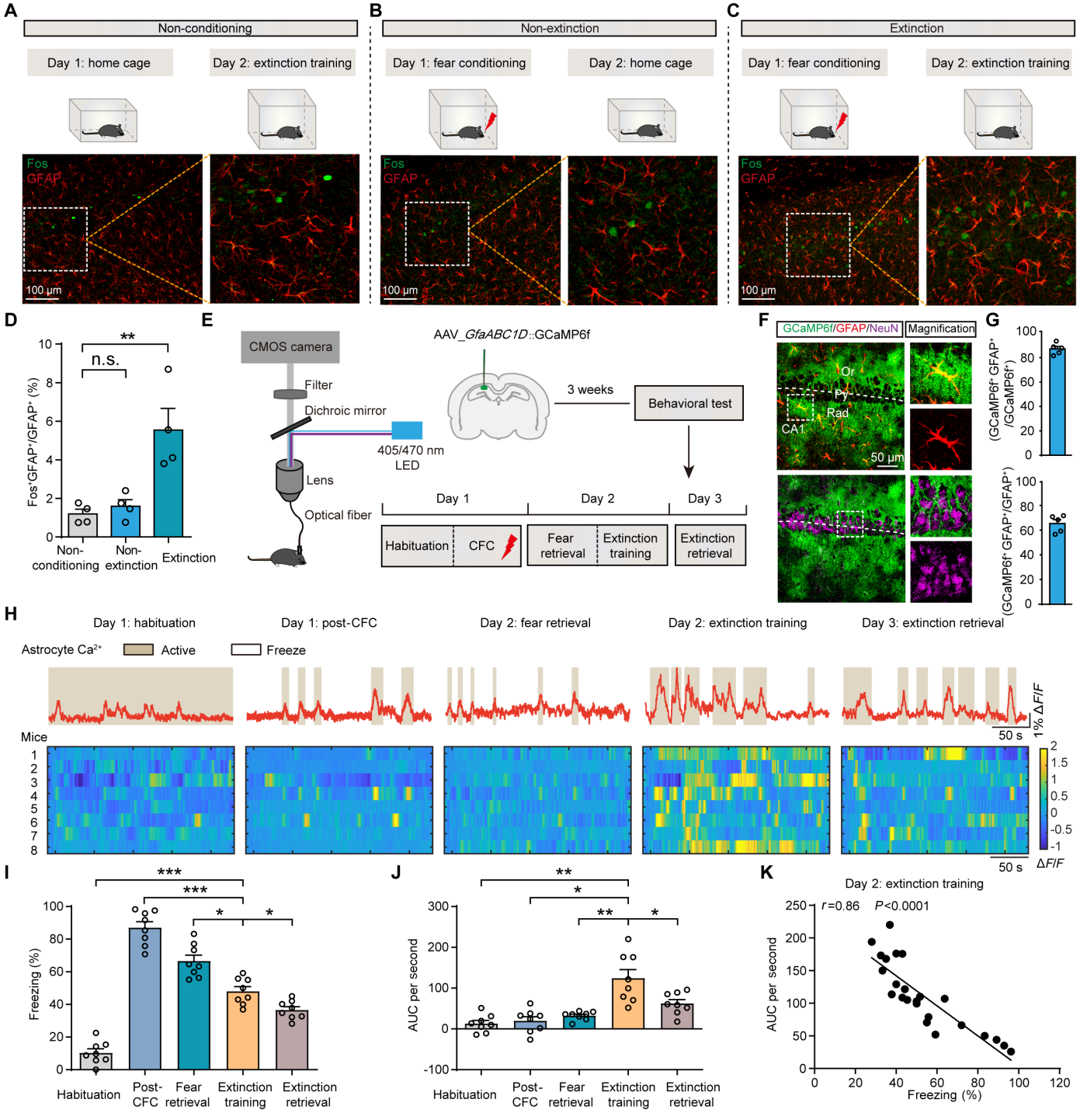


**Fig. 1. Hippocampal CA1 astrocyte de novo $Ca^{2+}$ response during contextual fear extinction.** (**A** to **C**) *Fos* and GFAP expression of non-conditioning, non-extinction, and extinction mice groups. Lightning bolt indicates footshocks. Scale bar, 100 μm. (**D**) Average percentage of $Fos^+$ astrocytes ($Fos^+GFAP^+/GFAP^+$ cells) ($n = 4$ per group). (**E**) Behavioral protocol for $Ca^{2+}$ recording. CFC, contextual fear conditioning. Lightning bolt indicates footshocks. (**F**) Confocal images showing colocalization of GCaMP6f labeling with the specific astrocytic marker GFAP (top), but not with the neuronal marker NeuN (bottom) (right, higher-magnification images from areas indicated by dashed squares; scale bar, 50 μm; Or, stratum oriens; Py, stratum pyramidale—dashed contour; Rad, stratum radiatum). (**G**) Specificity and efficiency of GCaMP6f expression in astrocytes ($n = 5$). (**H**) Top: Representative $Ca^{2+}$ $\Delta F/F$ traces of CA1 astrocytes. Beige, active state of mice; white, freeze state of mice. Bottom: Heatmaps reporting $\Delta F/F$ of astrocyte GCaMP6f signals ($n = 8$). (**I**) Quantification of freezing levels during different behavioral segments ($n = 8$). (**J**) Quantification of the area under the curve (AUC) per second for GCaMP6f signal in CA1 astrocytes during different behavioral segments ($n = 8$). (**K**) Negative linear correlation between the GCaMP6f AUC in CA1 astrocytes and the freezing level during extinction training ($n = 8$, 24 trials). Error bars show means ± SEM. $^*P < 0.05$, $^{**}P < 0.01$, $^{***}P < 0.001$, as determined by one-way ANOVA and Dunn's post hoc test [(I) and (J)].

cages without extinction training on day 2 (Fig. 1B, top). The non-conditioning group received the same protocol as the extinction group on days 2 and 3 except receiving no foot shocks on day 1 (Fig. 1A, top). On day 1, both extinction and non-extinction groups displayed robust freezing levels and have similar learning curve compared with the non-conditioning group (fig. S1B). On day 3, the extinction group exhibited a significant lower freezing level than the non-extinction group (fig. S1C). To understand how fear extinction influences astrocytes, we performed immunohistochemistry to detect activity-dependent expression of the immediate-early gene *Fos* in astrocytes after behavioral test on day 2. We harvested the brains of mice from each group and assessed the expression of *Fos*$^+$ cells among astrocytes across a host of brain regions, including PFC, thalamus, hippocampus, hypothalamus, amygdala, and periaqueductal gray (Fig. 1, A to C, bottom, and fig. S1D). Analysis revealed that in PFC and amygdala, the proportion of dually *Fos*$^+$ and GFAP$^+$ (glial fibrillary acidic protein–positive) cells of all GFAP$^+$ (*Fos*$^+$GFAP$^+$/GFAP$^+$) cells was significantly higher in both the non-extinction and extinction groups, indicating that astrocytes may be involved in both fear memory persistence and extinction (fig. S1D). In the dorsal hippocampal CA1 region (dCA1), however, the proportion of *Fos*$^+$GFAP$^+$/GFAP$^+$ cells was specifically and significantly higher solely in the extinction group when compared to non-extinction and non-conditioning groups (Fig. 1, A to D); no difference was observed between non-extinction and non-conditioning groups (Fig. 1, A to D). The proportion of *Fos*$^+$ cells among astrocytes in thalamus (paraventricular and central), hypothalamus, and periaqueductal gray showed no difference in the three groups (fig. S1D). These results demonstrate that de novo hippocampal dCA1 astrocyte activity (as assessed by the inducible transcription of *Fos*) was specifically induced during fear extinction.

Next, we performed in vivo $Ca^{2+}$ imaging using fiber photometry to dynamically record dCA1 astrocyte activity during CFC, followed by contextual fear extinction, and extinction memory retrieval (Fig. 1E). The genetically encoded $Ca^{2+}$ indicator GCaMP6f was specifically expressed in dCA1 astrocytes via injection of adeno-associated virus (AAV) with the astrocyte-specific *GfaABC1D* promoter driving the expression of the $Ca^{2+}$ indicator GCaMP6f (AAV_*GfaABC1D*::GCaMP6f). Costaining of cells expressing GCaMP6f in the hippocampus with GFAP, but not with neuronal NeuN, verified the specificity of GCaMP6f expression in astrocytes. We observed that 83.7% of the GCaMP6f-positive cells were GFAP-positive astrocytes (Fig. 1, F and G), and 62.0% of the GFAP-positive astrocytes in the CA1 region expressed GCaMP6f (Fig. 1, F and G). We did not detect any GCaMP6f signal in the nearby NeuN-stained neurons (Fig. 1F). Astrocyte intracellular $Ca^{2+}$ dynamics were recorded and analyzed during five behavioral segments: (i) during habituation to the conditioning chamber (day 1), (ii) post-CFC (day 1), (iii) fear retrieval (day 2), (iv) extinction training (day 2), and (v) extinction retrieval (day 3). The animal freezing level was significantly increased after CFC and decreased after fear extinction (Fig. 1I), while there was no alteration in astrocytic $Ca^{2+}$ responses immediately after CFC (Fig. 1J). However, the astrocytic responses enhanced on the following day during extinction training when mice were placed back into the conditioning context (Fig. 1, H and J). By comparison, when mice were relocated into context B (see Materials and Methods section for details), which is not relevant to conditioning, the enhanced astrocytic $Ca^{2+}$ responses dissipated (fig. S2, A and B). Moreover, in the non-conditioning control, astrocyte $Ca^{2+}$ activity remained at low levels during days 1 to 3 (fig. S2, C and D). During re-exposure in the novel object recognition (NOR) test (object A versus object B, or object A versus object C) or in the reward (sucrose) context, there were again no notable changes in astrocytic $Ca^{2+}$ responses (fig. S2, E to J). These results suggest that astrocytic responses are aversive experience–primed and are engaged when mice experience fear extinction. Further analysis revealed that astrocytic $Ca^{2+}$ responses were gradually increased during the extinction training. Compared with $Ca^{2+}$ signals during early fear retrieval, the signals were notably enhanced during later extinction period (fig. S2, K and L), strengthening the specific $Ca^{2+}$ signaling during the fear extinction training. In addition, astrocytic $Ca^{2+}$ responses were inversely correlated with the freezing levels during fear extinction (Fig. 1K), suggesting a possible pro-extinction role of the astrocytic $Ca^{2+}$ responses. Moreover, astrocytic $Ca^{2+}$ responses during extinction retrieval were significantly smaller than those during the extinction training when the fear level is higher (Fig. 1, H and J), suggesting that the strength of astrocytic $Ca^{2+}$ responses is dependent on the fear level. Together, these results indicate astrocytes as an active participant in fear extinction.

## CA1 astrocytes modulate contextual fear extinction

Next, we investigated the potential causative role of astrocytes in fear extinction. To test whether astrocyte $Ca^{2+}$ activity is required for fear extinction, we used an AAV expressing mCherry-conjugated human plasma membrane $Ca^{2+}$ adenosine triphosphatase (ATPase) 2 (referred for simplicity as hPMCA2w/b), and driven by *GfaABC1D* promoter, to attenuate astrocyte activity as previously reported (*30*, *31*) (Fig. 2, A and B). We verified the specific hPMCA2w/b expression in GFAP$^+$ astrocytes (Fig. 2C, top), while no expression was detected in nearby NeuN$^+$ neurons (Fig. 2C, bottom). We recorded dCA1 astrocyte $Ca^{2+}$ signaling using virally expressed GCaMP6f in these cells and fiber photometry (Fig. 2, D and E). We observed that the de novo astrocytic $Ca^{2+}$ response during fear extinction significantly diminished in the hPMCA2w/b group when compared to the control group of mice (Fig. 2, D and E). In the behavioral test, hPMCA2w/b mice exhibited significantly slower extinction curve on day 2 and higher freezing level on day 3 (Fig. 2, F to I). These results indicate that de novo induced hippocampal CA1 astrocyte $Ca^{2+}$ responses are necessary for fear extinction.

We and others have previously demonstrated that optogenetic and chemogenetic activation induces $Ca^{2+}$ elevations in astrocytes (*18*, *19*, *22*, *23*, *32*–*35*). As hPMCA2w/b expressed in astrocytes chronically and could not be able to inhibit astrocytic $Ca^{2+}$ signaling with temporal precision, to investigate the causative role of hippocampal CA1 astrocytes in fear extinction, we expressed channelrhodopsin 2 (ChR2) conjugated with enhanced green fluorescent protein (EGFP) in astrocytes via viral injection of AAV_*GfaABC1D*::ChR2-EGFP, into the dCA1 region, while in control we used viral expression of EGFP (Fig. 3A). We verified the specificity of ChR2-EGFP expression in GFAP$^+$ astrocytes (Fig. 3B). We observed that 95.5% of the ChR2-EGFP$^+$ cells were GFAP$^+$ astrocytes and 69.0% of the GFAP$^+$ astrocytes in CA1 expressed ChR2-EGFP (Fig. 3, B and C). We did not detect ChR2-EGFP signal in nearby NeuN$^+$ CA1 neurons (Fig. 3B). To verify the functional response of astrocytes to optogenetic manipulation, we performed $Ca^{2+}$ imaging in hippocampal slices. We loaded astrocytes with a $Ca^{2+}$ dye (Rhod-2 AM) and observed that light stimulation reliably induced robust $Ca^{2+}$ elevation in astrocytes expressing ChR2-EGFP compared with EGFP (fig. S3,

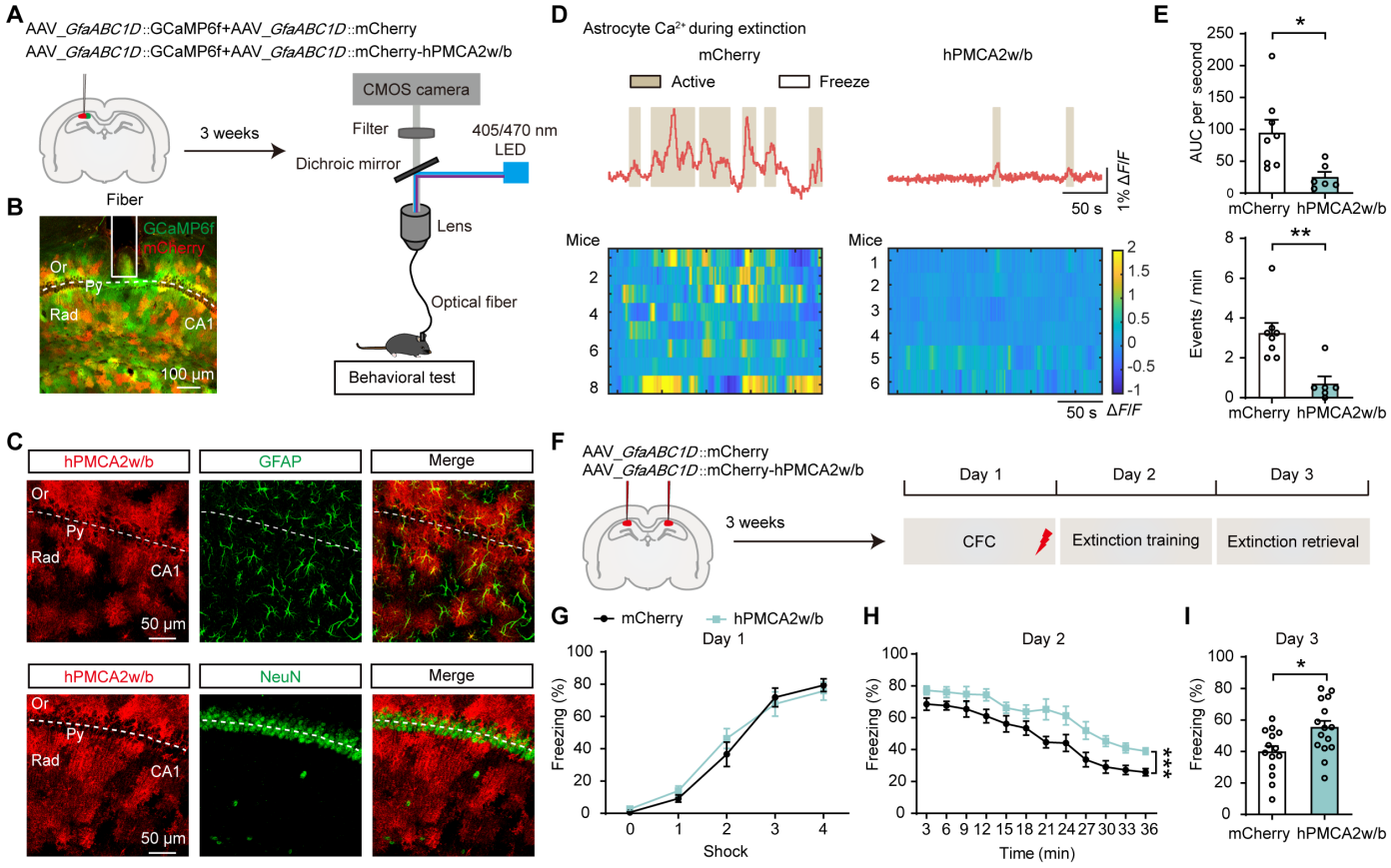


**Fig. 2. Inhibition of astrocytic $Ca^{2+}$ signaling impairs contextual fear extinction.** (**A**) Diagram of viral microinjection in the CA1 region of mice and fiber photometry recording. (**B**) Confocal images showing viral expression. Scale bar, 100 μm. Abbreviations and dashed contour as in Fig. 1F. (**C**) Confocal images showing colocalization of mCherry-hPMCA2w/b (below as hPMCA2w/b from simplicity) labeling with GFAP, but not with NeuN. Scale bar, 50 μm. (**D**) Top: Representative astrocytic $Ca^{2+}$ Δ*F*/*F* traces of mCherry and hPMCA2w/b mice during fear extinction ($n = 6$ to 8 per group). Beige, active state of mice; white, freeze state of mice. Bottom: Heatmaps reporting Δ*F*/*F* of astrocyte GCaMP6f signals. (**E**) Top: Quantification of the GCaMP6f AUC in CA1 astrocytes of mCherry and hPMCA2w/b mice during fear extinction. Bottom: Frequency of calcium events for the mCherry and hPMCA2w/b group mice. (**F**) Diagram of viral microinjection in the CA1 region of mice and behavioral test. (**G**) Freezing levels of mCherry and hPMCA2w/b mice during fear conditioning on day 1 ($n = 14$ to 15 per group). (**H**) Extinction curve of mCherry and hPMCA2w/b mice during fear extinction training on day 2. (**I**) Freezing levels of mCherry and hPMCA2w/b mice during extinction retrieval test on day 3. Error bars show means ± SEM. $^*P < 0.05$, $^{***}P < 0.001$, as determined by unpaired *t* test [(E) and (I)] and two-way ANOVA followed by Bonferroni's multiple comparisons test (H).

A to C). We quantified $Ca^{2+}$ events in visual field and showed significant increase in ChR2-EGFP–expressing astrocytes (fig. S3D).

Mice underwent a 3-day contextual fear extinction protocol (Fig. 3D). Starting 3 min after the onset of fear extinction on day 2, a 60-s blue laser light pulse was delivered repeatedly at 60-s intervals to excite ChR2 expressed in dCA1 astrocytes. This optogenetic activation of astrocytes enhanced fear extinction learning on day 2 and decreased freezing level of mice on days 3 and 10 (Fig. 3D). To further differentiate the role of astrocytes in fear extinction training and fear extinction memory retrieval, we optogenetically activated dCA1 astrocytes during fear extinction memory retrieval on day 3 and found that this activation of astrocytes did not affect the freezing level (Fig. 3E).

To verify the role of astrocytes in fear extinction as implied by optogenetics, we also used chemogenetic activation of astrocytes virally transfected with a modified human M3 muscarinic receptor (hM3Dq) conjugated with mCherry, the expression of which was driven by the *GfaABC1D* promoter, while in control we used viral expression of mCherry (Fig. 3F). We confirmed that 91.8% of the hM3Dq-mCherry$^+$ astrocytes were GFAP$^+$ and 69.8% of the GFAP$^+$ astrocytes in the CA1 region expressed hM3Dq-mCherry (Fig. 3, G and H). We did not detect mCherry signal in NeuN$^+$ CA1 neurons (Fig. 3G). To verify chemogenetic activation of astrocyte activity (*22*, *23*), we virally expressed hM3Dq-mCherry (AAV_*GfaABC1D*::hM3Dq-mCherry) and GCaMP6f (AAV_*GfaABC1D*::GCaMP6f) in astrocytes (fig. S4A). We used fiber photometry to record CA1 astrocyte $Ca^{2+}$ activity with saline or clozapine-N-oxide (CNO) injection. Intracranial microinjection of CNO (10 μM) in the CA1 robustly increased astrocyte $Ca^{2+}$ activity (fig. S4, B and C). Moreover, CNO application by intraperitoneal (IP) injection (1 mg/kg) also triggered an increase in intracellular $Ca^{2+}$ and in the frequency of $Ca^{2+}$ events (fig. S4, D to F).

To investigate the effect of astrocytic activation on fear extinction, mice were injected with saline (1 mg/kg, hM3Dq + saline, IP) or CNO (1 mg/kg, mCherry + CNO, hM3Dq + CNO, IP) 30 min before extinction training on day 2. Chemogenetic activation of astrocytes during extinction training also enhanced fear extinction learning on day 2 and decreased freezing level on days 3 and 10 (Fig. 3I).

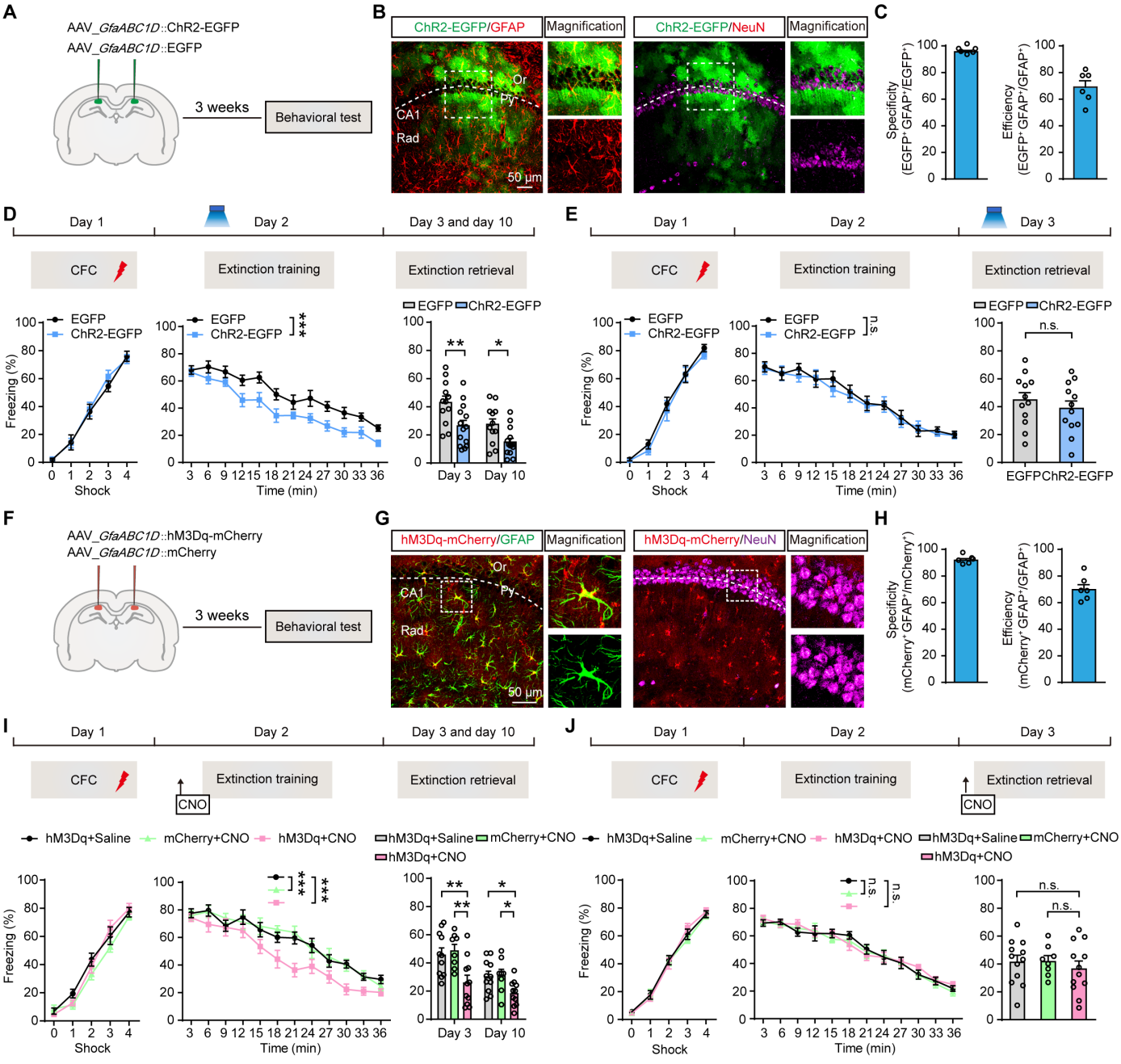


**Fig. 3. Activation of astrocyte facilitates contextual fear extinction.** (**A** and **F**) Diagram of bilateral viral microinjection in CA1 regions and behavioral test. (**B**) Confocal images showing colocalization of ChR2-EGFP labeling with GFAP, but not with NeuN (higher-magnification images from areas indicated by dashed squares; scale bar, 50 μm). Abbreviations and dotted contour [here and in (G)] as in Fig. 1F. (**C**) Specificity and efficiency of ChR2-EGFP expression in astrocytes ($n = 6$). (**D**) Optogenetic activation, indicated by a blue flashlight, of CA1 astrocytes during extinction training–enhanced fear extinction training and decreased fear memory ($n = 12$ to 14 per group). (**E**) Optogenetic activation of CA1 astrocytes during extinction retrieval did not affect fear extinction memory ($n = 12$ per group). (**G**) Confocal images showing colocalization of hM3Dq-mCherry labeling with GFAP, but not with NeuN (scale bar, 50 μm). (**H**) Specificity and efficiency of hM3Dq-mCherry expression in astrocytes ($n = 6$). (**I**) Chemogenetic activation of CA1 astrocytes during extinction training–enhanced fear extinction training and decreased fear memory ($n = 8$ to 11 per group). (**J**) Chemogenetic activation of CA1 astrocytes during extinction retrieval did not affect fear extinction memory ($n = 8$ to 12 per group). Error bars show means ± SEM. $^*P < 0.05$, $^{**}P < 0.01$, $^{***}P < 0.001$, as determined by two-way ANOVA followed by Bonferroni's multiple comparisons test on day 2 [(D), (E), (I), and (J)], unpaired *t* test on days 3 and 10 [(D), (E), and (I)], and one-way ANOVA and Dunn's post hoc test on day 3 (J).

In contrast, chemogenetic activation of astrocytes during extinction memory retrieval did not affect the freezing level (Fig. 3J). We did not observe an effect of astrocyte chemogenetic activation on the baseline freezing levels in context B that was distinct from the fear conditioning context (fig. S5, D and E). In addition, activation of ChR2/hM3Dq-expressing astrocytes did not affect the locomotion or anxiety level of mice in the open-field test (fig. S5, A to C and F to H). These results demonstrated that the enhanced astrocyte activation, using photo- or chemo-actuators, in the dCA1 region accelerates fear extinction.

### ACh signal precedes and correlates with astrocytic $Ca^{2+}$ activity during fear extinction

The alterations in $Ca^{2+}$ activity in hippocampal astrocytes during fear extinction led us to examine the causes of the astrocytic $Ca^{2+}$ response. Astrocytes express various G protein–coupled receptors and ion channels, which respond to neurotransmitters or neuromodulators released by and spilled over from synaptic activity, resulting in astrocyte $Ca^{2+}$ elevations (*17*, *36*). We virally expressed sensors for extracellular ACh (AAV_*GfaABC1D*::gACh4h), adenosine triphosphate (ATP) (AAV_*GfaABC1D*::cATP1.0), or serotonin [5-hydroxytryptamine (5-HT)] (AAV_*hSyn*::5-HT3.0) (*37*). Viruses were injected into the CA1 region separately, and extracellular neurotransmitters signals were recorded using fiber photometry (Fig. 4, A and B, and fig. S6, A to C).

We investigated extracellular levels of ACh, 5-HT, or ATP in the CA1 region during fear extinction. There were no notable changes in ATP and 5-HT signals during extinction training on day 2 (fig. S6, D, E, G, and H). As a positive control, we tested the activity of cATP1.0 and 5-HT3.0 sensors by inducing either generalized seizures by pentylenetetrazole or providing footshock stimulation, respectively. In response, we observed significant increases in ATP or 5-HT signals indicating proper operation of these neurotransmitter sensors (fig. S6, F and I).

Quite the contrary, we found that ACh signal in astrocytes increased significantly during extinction training as compared to those signals during habituation, after CFC and fear retrieval (Fig. 4, C and D). When mice were placed on day 2 in context B, no increase of ACh signal was observed (fig. S7, A and B). In the nonconditioning group, ACh signal remained at similarly low levels during days 1 to 3 (fig. S7, C and D). In the NOR experiments, ACh signals showed no notable change during novel versus old objects recognition on days 1 and 2 (fig. S7, E to G). Moreover, in the reward (sucrose) experiment, ACh signal showed no notable change (fig. S7, H to J). Moreover, ACh signal during extinction retrieval was significantly smaller than that during the extinction training when the fear level is higher (Fig. 4, C and D). Further analysis revealed the freezing levels during fear extinction were inversely correlated with ACh signals (Fig. 4E). These data demonstrated that the de novo increase in extracellular levels of ACh occurs specifically during fear extinction in a fear-experience and context-dependent manner; these findings echo those of astrocytic $Ca^{2+}$ responses during fear extinction. We also used an ACh-insensitive sensor as control (fig. S8, A and B). There were no substantial changes in ACh signals during different behavioral segments compared with gACh4h signals (fig. S8, C to E).

To further determine the relationship between increased extracellular ACh levels and astrocytic $Ca^{2+}$ activity in the dCA1 region, we simultaneously virally expressed the gACh4h sensor and spectrally compatible jRGECO1a (red emission) in astrocytes, and recorded their signals (Fig. 4F). We verified the specific jRGECO1a expression in $S100\beta^+$ astrocytes, while no expression was detected in nearby $NeuN^+$ neurons (Fig. 4G). We found that extracellular ACh and astrocyte intracellular $Ca^{2+}$ signals were temporally coupled and positively correlated, with the extracellular ACh signal raise preceding astrocytic $Ca^{2+}$ elevations by ~2 s (Fig. 4, H to J). These findings suggest that increased extracellular ACh levels, presumably due to synaptic activity and spillover (studied next), stimulate astrocyte $Ca^{2+}$ dynamics during fear extinction.

### pBF cholinergic projections activate astrocytes through nicotinic ACh receptors

Previous studies reported that the cholinergic inputs to the hippocampus originated mostly from the anterior basal forebrain (aBF), such as the medial septum and diagonal bands of Broca (MS and DBB) (*38*–*40*). Here, in the retrograde tracing experiments, using choline acetyltransferase (ChAT)–IRES–Cre mice and hippocampal injection of a virus (AAV2/2retro_*hEF1a*::DIO-EYFP) with *hEF1a* promotor driving Cre-dependent *EYFP* (enhanced yellow fluorescent protein) expression, we quantified the number of cholinergic neurons retrogradely labeled from the dCA1 region to the BF (in its anterior-posterior axis). The number of retrogradely labeled cholinergic cells was lower in the aBF, in particular in the MS, vertical limb of DBB (vDBB), and horizontal limb of DBB (hDBB), whereas the number of cholinergic neurons was higher in the pBF (Fig. 5, A to C). In the anterograde tracing experiment in ChAT-IRES-Cre mice and using a virus (AAV_*hSyn*::DIO-EYFP), EYFP-labeled pBF projections were found in the dCA1 region with the cholinergic axon terminals scattered around the astrocyte marker GFAP, showing the close anatomical proximity of astrocytes with pBF cholinergic projections (Fig. 5D).

To test whether the pBF cholinergic input drives astrocytic $Ca^{2+}$ response in the dCA1 region, we virally expressed the Cre-dependent red-light gated channelrhodopsin, ChrimsonR-tdTomato (AAV_*hSyn*::FLEX-ChrimsonR-tdTomato), in the pBF cholinergic neurons and GCaMP6f in dCA1 astrocytes of ChAT-IRES-Cre mice (Fig. 5E). We then optogenetically activated cholinergic axon terminals in the dCA1 region and used fiber photometry to record the astrocytic $Ca^{2+}$ responses. Photoactivation of ChrimsonR in cholinergic terminals (638-nm laser, 10 ms/pulse, 10 Hz for 10 s) induced astrocyte $Ca^{2+}$ responses in home cage mice on day 1, and astrocyte response was augmented in mice receiving the extinction training on day 2 (Fig. 5, F and G), indicating a plasticity in this neuron-astrocyte signaling.

We then identified the ACh receptor type [nicotinic (nAChRs) and/or muscarinic (mAChRs)] mediating the augmented astrocyte $Ca^{2+}$ responses in ChAT-IRES-Cre mice that received extinction training on day 2. The ChrimsonR light-evoked astrocyte $Ca^{2+}$ response was blocked after injection of nAChR antagonist [mecamylamine hydrochloride (MECA), 0.1 mM] but not mAChR antagonist atropine (0.1 mM) in the dCA1 region (Fig. 5, H and I), each antagonist at volume of 1 μl. Further, the specific α4 subunit or α7 subunit of nAChR antagonist dihydro-β-erythroidine hydrobromide (DHβE; 0.1 mM) or methyllycaconitine (MLA; 0.1 mM), respectively and separately (each at volume of 1 μl), blocked the ChrimsonR light-evoked astrocyte $Ca^{2+}$ response (Fig. 5, H and I); there was a trend of additive blocking effect in the presence of both DHβE and MLA (Fig. 5, H and I). Of note, the use of

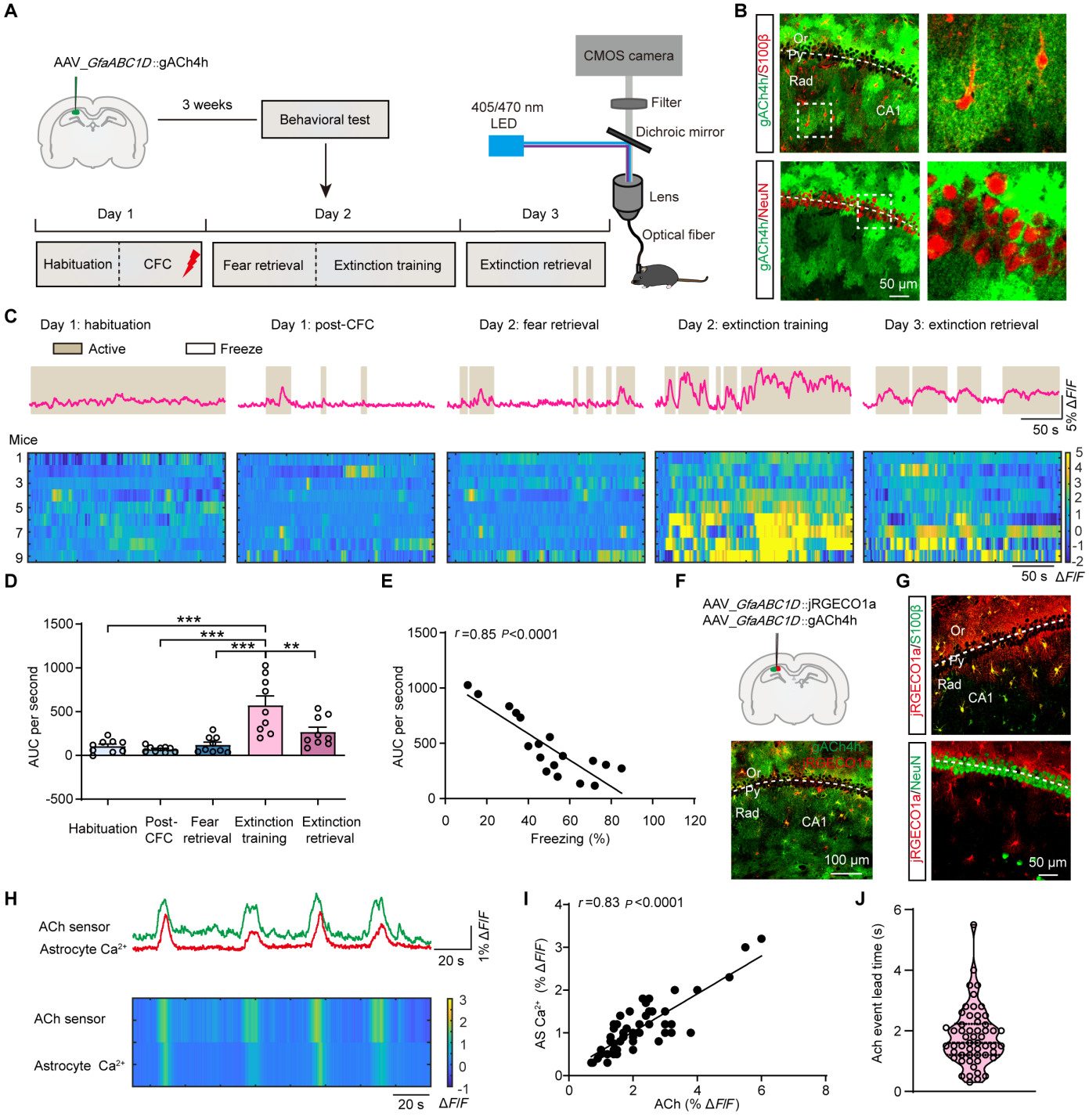


**Fig. 4. ACh signal precedes and correlates with astrocytic $Ca^{2+}$ activity during contextual fear extinction.** (**A**) Behavior protocol for ACh sensor (gACh4h) recording. (**B**) Representative images showing ACh sensor–specific expression on astrocytes and colocalization of gACh4h labeling with the specific astrocytic marker S100β, but not with NeuN. Scale bar, 50 μm. (**C**) Top: Representative Δ*F*/*F* traces of ACh sensor in the CA1 region. Beige, active state of mice; white, freeze state of mice. Bottom: Examples of heatmaps reporting on Δ*F*/*F* of ACh sensor in the CA1 region ($n = 9$). (**D**) Quantification of the AUC of ACh signal during different behavioral segments ($n = 9$). (**E**) Negative linear correlation between the AUC of ACh signal in the CA1 region and the freezing level during extinction training (nine mice, 18 trials). (**F**) Expression of the ACh sensor and astrocyte jRGECO1a in hippocampal slices. Scale bar, 100 μm. (**G**) Confocal images showing colocalization of jRGECO1a labeling with S100β, but not with NeuN. Scale bar, 50 μm. (**H**) Representative Δ*F*/*F* traces and heatmaps of astrocyte $Ca^{2+}$ and extracellular ACh signals recorded simultaneously. (**I**) Positive linear correlation between extracellular ACh and astrocyte $Ca^{2+}$ signals (nine mice, 54 trials). (**J**) The rise of extracellular ACh signal preceded the increase of astrocyte $Ca^{2+}$ signal. Error bars show means ± SEM. $^{**}P < 0.01$, $^{***}P < 0.001$, as determined by one-way ANOVA and Dunn's post hoc test (D). Lightning bolt, abbreviations, and dashed contour as in Fig. 1.

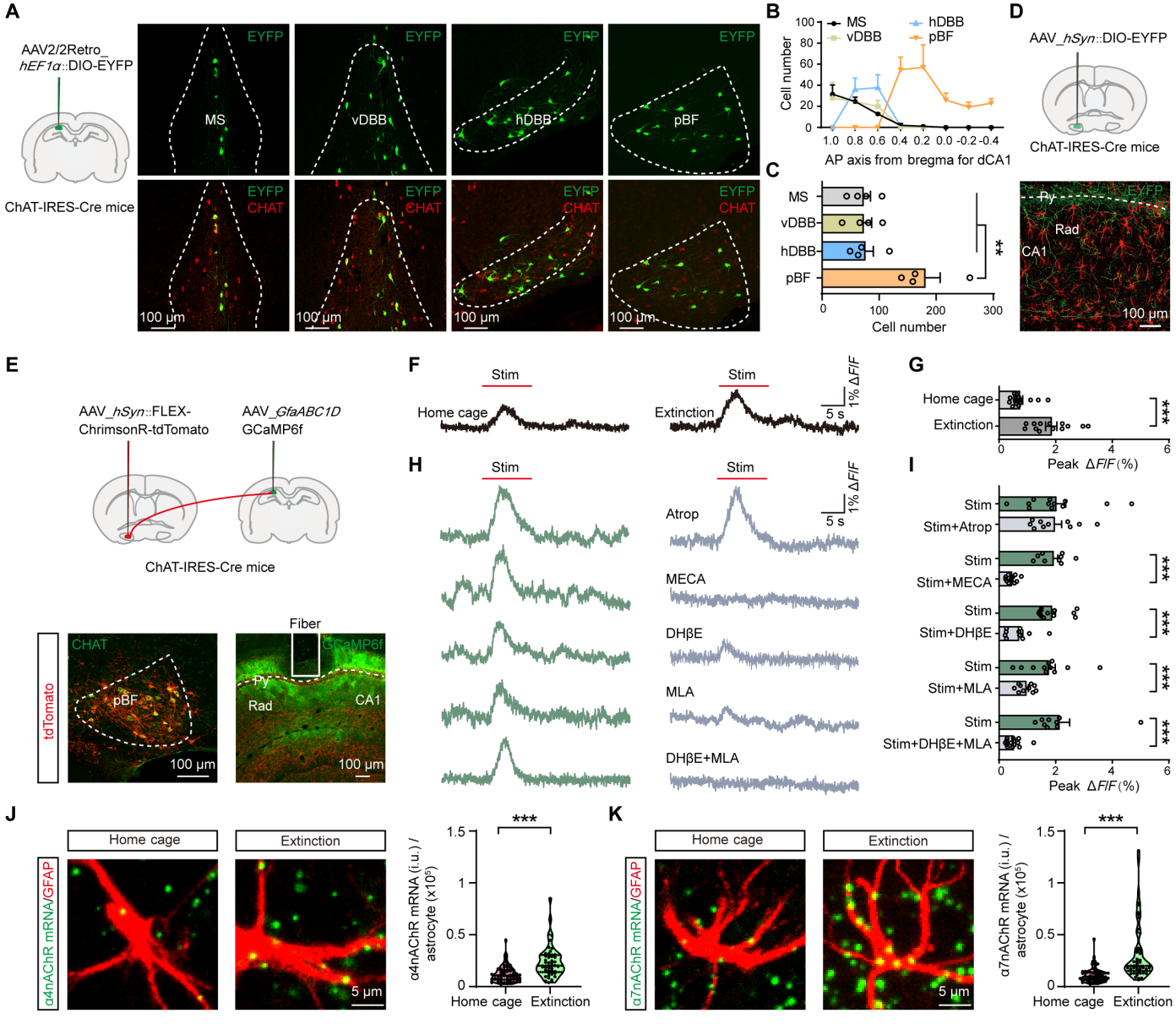


**Fig. 5. pBF cholinergic projections activate astrocytes through nAChRs.** (**A**) Retrograde tracing of cholinergic neurons innervating dCA1 region, shown to express EYFP in BF subregions: MS, vDBB, hDBB, and pBF (scale bars, 100 μm). ChAT, cholinergic neuron marker. (**B**) Traces indicate EYFP$^+$ neurons in BF subregions across the anterior-posterior axis (AP axis: 1.0 mm to −0.4 mm from bregma, $n = 4$). (**C**) Average EYFP$^+$ neuron count in BF subregions. (**D**) Anterograde tracing of pBF cholinergic neurons and EYFP expression in the CA1 region (scale bar, 100 μm). (**E**) Viral expression of ChrimsonR in pBF cholinergic neurons and GCaMP6f in dCA1 astrocytes (scale bar, 100 μm). (**F**) Representative GCaMP6f signals in dCA1 evoked by optogenetic activation of ChAT$^+$ neurons (638-nm laser, 10 ms/pulse, 10 Hz for 10 s) alone in home cage and extinction training. (**G**) Quantification of evoked astrocyte signals in (F) ($n = 5$, 14 to 16 trials per group). (**H**) Representative GCaMP6f signals. The signal is blocked by nAChR antagonist (MECA, $n = 4$, 9 to 12 trials per group) but not by mAChR antagonist [atropine (Atrop), $n = 5$, 10 trials per group]; specific nAChRα4 (DHβE, $n = 7$, 10 to 13 trials per group) or nAChRα7 subunit antagonists (MLA, $n = 4$, 9 to 10 trials per group), respectively, or combined (DHβE + MLA, $n = 5$, 9 to 12 trials per group) blocked the evoked astrocyte $Ca^{2+}$ response. (**I**) Quantification of astrocyte signals before and after drug application in (H). (**J** and **K**) nAChRα4 or nAChRα7 subunit mRNA expression [in intensity units (i.u.)] in dCA1 astrocytes from home cage and extinction treatment mice (scale bar, 5 μm). Error bars show means ± SEM. $^{**}P < 0.01$, $^{***}P < 0.001$, as determined by one-way ANOVA and Bonferroni's post hoc test (C) and unpaired *t* tests [(G) and (I) to (K)].

lower concentrations of combined DHβE and MLA blockers may allow for a notable additive effect, which is beyond the scope of the present study, and it awaits future studies. Thus, the response of astrocyte to ACh is mediated by α4- and α7-containing nAChRs.

We further quantified mRNA transcripts for α4 and α7 nAChR subunits using fluorescence probes and their location in astrocytes assigned based on the GFAP signal. In dCA1 astrocytes of mice after fear extinction on day 2, as compared to home caged day 1 mice, there were significant increases in mRNA for both α4 and α7 nAChR subunits (Fig. 5, J and K). These data indicate that fear extinction results in an up-regulation of α4 and α7 nAChR subunits in astrocytes of the dCA1 region; these subunits mediate enhanced $Ca^{2+}$ activity in hippocampal astrocytes driven by nearby pBF cholinergic terminals.

To examine whether local neuronal activity in the hippocampus contributes to the astrocyte $Ca^{2+}$ dynamics during fear extinction, we virally expressed in hippocampal neurons a modified form of the human M4 muscarinic (hM4) receptor–mCherry (AAV_*hSyn*::hM4Di-mCherry), which can be activated by CNO to exert its inhibitory action on neuronal activity, along with viral expression of GCaMP6f in hippocampal astrocytes to image their $Ca^{2+}$ dynamics (fig. S9, A and B). We found no differences in the average amplitude of astrocyte $Ca^{2+}$ signals during fear extinction following administration of either saline or CNO (fig. S9, C and D). These results indicate that local neuronal activity does not contribute to astrocyte $Ca^{2+}$ responses, suggesting that the ACh signaling from pBF directly causes astrocyte $Ca^{2+}$ responses in the dCA1 region of the hippocampus during fear extinction, which we directly address next.

### pBF cholinergic inputs to CA1 astrocytes mediate control of fear extinction

Previous research found that cholinergic neuronal lesions in the aBF, in particular MS or vDBB, induced contextual fear memory generalization and impaired acquisition of fear extinction (*41*). Additionally, stimulation of cholinergic terminals within the basolateral amygdala during cued fear conditioning slowed fear extinction (*42*). Consequently, we examined whether pBF cholinergic inputs to CA1 astrocytes mediate control of fear extinction. We expressed Cre-dependent axon-GCaMP6s in pBF cholinergic neurons of ChAT-IRES-Cre mice (using AAV_*EF1a*::DIO-axon-GCaMP6s) and recorded GCaMP6s fluorescence in the CA1 region using fiber photometry (fig. S10, A and B). Similar to the extracellular ACh level increase, the $Ca^{2+}$ activity of cholinergic axon terminals was significantly increased during fear extinction (fig. S10, C and D).

To further study the role of cholinergic pBF inputs to the CA1 region in fear extinction, we Cre-dependently expressed ChR2-EYFP (using AAV_*EF1a*::DIO-ChR2-EYFP) in pBF cholinergic neurons of ChAT-IRES-Cre mice (fig. S11, A and B) and found that optogenetic activation of cholinergic terminals in the CA1 region significantly enhanced fear extinction on day 2 and reduced freezing level on day 3 as compared to control of ChAT-IRES-Cre mice whose pBF cholinergic neurons Cre-dependently expressed EYFP (fig. S11C). We then assessed whether CA1 astrocytes are required for pBF cholinergic activation–induced enhancement of fear extinction. We expressed mCherry-hPMCA2w/b (using injection of AAV_*GfaABC1D*::mCherry-hPMCA2w/b) on CA1 astrocytes to decrease astrocytic $Ca^{2+}$ activity, which blocked the effect of cholinergic terminal activation on fear extinction when compared to controls in which astrocytes expressed the fluorescent marker mCherry (fig. S11C). These results indicate that pBF cholinergic input to the CA1 region induces fear extinction facilitation through the activation of astrocytes.

To further evaluate the subtype of cholinergic receptors in astrocytes mediating this phenomenon, we knocked down the level of α4 or α7 nAChR by targeting CA1 astrocytes with AAV_*GfaABC1D*::RNAi(α4nAChR)-mCherry or AAV_*GfaABC1D*::RNAi(α7nAChR)-mCherry, separately, and Cre-dependently expressed ChR2-EYFP in pBF cholinergic neurons of ChAT-IRES-Cre mice. We verified the specificity and efficiency of RNAi(α4nAChR)-mCherry and RNAi(α7nAChR)-mCherry expression in astrocytes (fig. S12, A to D). The knockdown efficiency of RNAi was confirmed by using in situ hybridization for the examination of *Chrna4* and *Chrna7* gene transcripts (fig. S12, E to H). We verified that knockdown of α4 or α7 nAChR in astrocytes did not affect their expression in neurons (fig. S12, I to L).

To further investigate whether knockdown of astrocytic α4 or α7 nAChR affects astrocyte activity, we Cre-dependently expressed ChrimsonR-tdTomato in the pBF cholinergic neurons, GCaMP6f paired with mCherry or RNAi(α4nAChR)-mCherry or RNAi(α7nAChR)-mCherry in dCA1 astrocytes of ChAT-IRES-Cre mice (fig. S12, M and N). Photoactivation of dCA1 cholinergic terminals reliably induced astrocyte $Ca^{2+}$ responses (mCherry group), which is not observed in RNAi(α4nAChR)-mCherry or RNAi(α7nAChR)-mCherry group mice (fig. S12, O and P). These results suggested that knockdown of astrocytic α4 or α7 nAChR blocked cholinergic activation–induced astrocyte $Ca^{2+}$ responses.

We then assessed the impact of astrocytic α4 or α7 nAChR on fear extinction (fig. S13A). Compared to the ChR2-EYFP group (ChR2-EYFP + mCherry), which displayed decrease in freezing level as compared to EYFP control, optogenetic cholinergic terminal activation paired with astrocytic α4 nAChR or α7 nAChR knockdown reversed the freezing level to that comparable of the EYFP group on day 2 (fig. S13B). The decrease in freezing level caused by photostimulation of the ChR2-EYFP group on day 3 was also reversed by astrocytic α4 nAChR or α7 nAChR knockdown (fig. S13B), suggesting the necessity for astrocytic α4 and α7 subunits containing nAChR for cholinergic terminal activation-induced fear extinction facilitation.

To assess whether the cholinergic input is required for the de novo astrocyte $Ca^{2+}$ responses and their effect on fear extinction, we ablated pBF cholinergic (ChAT positive) neurons in ChAT-IRES-Cre mice by viral delivery of Cre-depended taCaspase 3 (AAV_*hEF1a*::FLEX-taCasp3) into the pBF, while control (no ablation) mice virally expressed mCherry in pBF cholinergic neurons (AAV_*hEF1a*::FLEX-mCherry) (Fig. 6A). Four weeks post-injection of viruses, pBF ChAT-positive neurons were almost absent in the taCasp3-injected mice, while there was no detectable loss of ChAT-positive cells in MS, vDBB, and hDBB, i.e., aBF (Fig. 6, B and C); in mCherry mice, ChAT neurons were omnipresent in these brain areas, however. We next assessed dCA1 astrocyte $Ca^{2+}$ dynamics during fear extinction and found that CA1 astrocyte $Ca^{2+}$ activity (as per viral injection of AAV_*GfaABC1D*::GCaMP6f) decreased significantly in the pBF ChAT neuron–ablated mice (Fig. 6, D and E). In the behavioral test, compared to controls, pBF ChAT neuron–ablated mice showed significantly slower extinction curve on day 2 and higher freezing level on day 3 (Fig. 6, F to I; compare mCherry + EGFP control versus taCasp3 + EGFP groups), while photoactivation of astrocytes reversed the freezing level in pBF ChAT neuron–ablated mice when compared to those of controls on both day 2 (Fig. 6H)

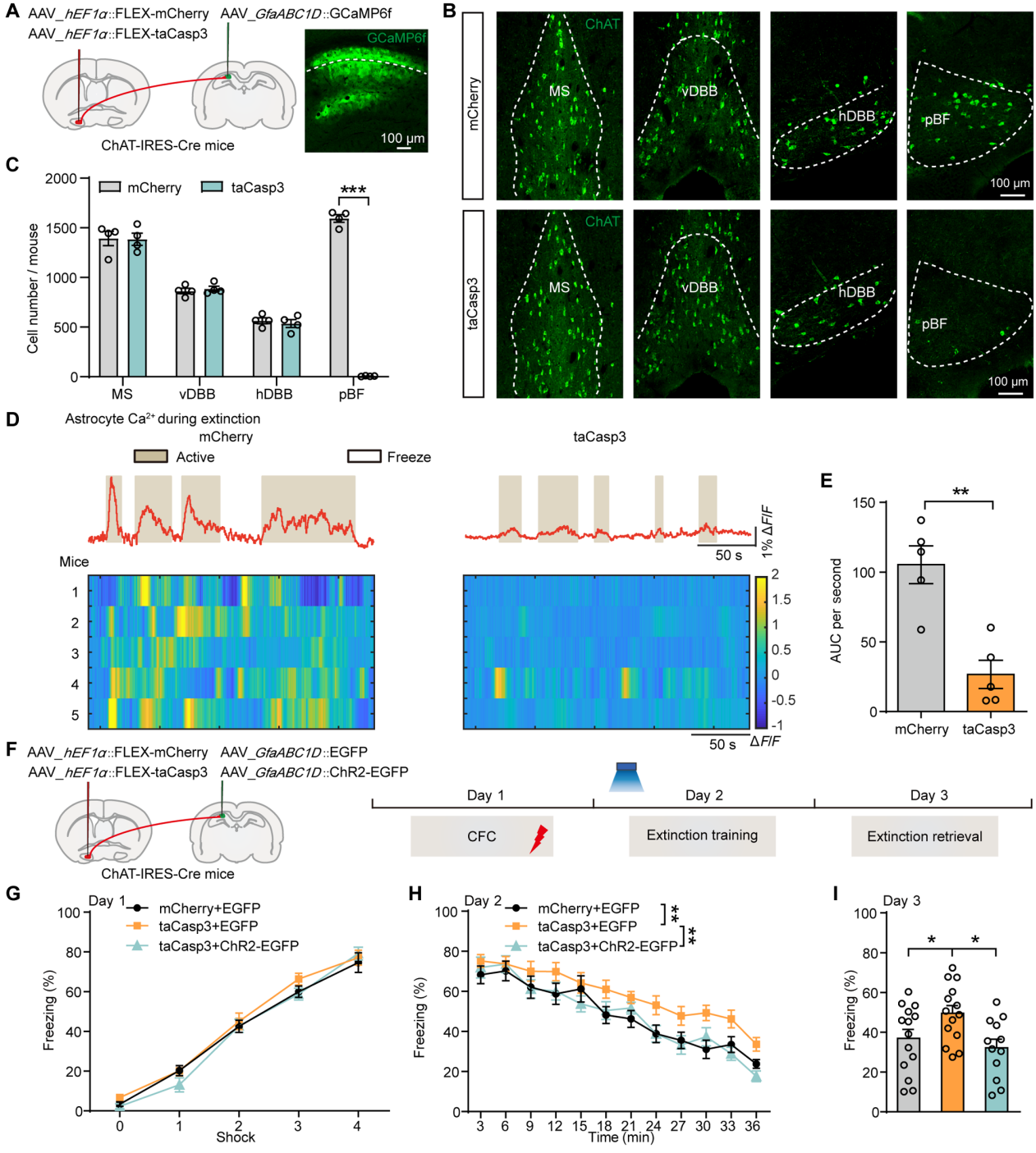


**Fig. 6. Ablation of pBF cholinergic neurons decreases dCA1 astrocyte $Ca^{2+}$ activity and impairs fear extinction.** (**A**) Diagram of viral microinjection in the pBF and dCA1 region of ChAT-IRES-Cre mice. Right: GCaMP6f expression in the CA1 region. Scale bar, 100 μm. (**B**) Cholinergic neurons in MS, vDBB, hDBB, and pBF with mCherry and taCasp3 viral microinjection ($n = 4$ per group). Scale bar, 100 μm. Contours as in Fig. 5. (**C**) Quantification of cholinergic neuron numbers in MS, vDBB, hDBB, and pBF indicates specificity of ablation of neurons in pBF. (**D**) Top and bottom: Representative $\Delta F/F$ traces and heatmaps of astrocyte GCaMP6f signals, respectively, of mCherry and taCasp3 mice during fear extinction ($n = 5$ per group). Beige, active state of mice; white, freeze state of mice. (**E**) Quantification of the GCaMP6f AUC in CA1 astrocytes. (**F**) Diagram of viral microinjection and behavioral test. (**G**) Similar freezing levels of control, pBF cholinergic neurons depleted with astrocytes expressing EGFP mice, and pBF cholinergic neurons depleted coupled with activation of ChR2-EGFP–expressing astrocytes in mice during fear conditioning on day 1 ($n$ = 12 to 15 per group). (**H**) Extinction curve of taCasp3 + EGFP mice is retarded when compared to mCherry + EGFP and taCasp3 + ChR2-EGFP groups during fear extinction training on day 2. (**I**) Freezing levels of taCasp3 + EGFP mice are increased when compared to mCherry + EGFP and taCasp3 + ChR2-EGFP groups during extinction retrieval memory test on day 3. Error bars show means ± SEM. $^*P < 0.05$, $^{**}P < 0.01$, $^{***}P < 0.001$, as determined by unpaired $t$ test [(C) and (E)], two-way ANOVA followed by Bonferroni's multiple comparisons test (H), and one-way ANOVA and Dunn's post hoc test (I).

and day 3 (Fig. 6I) (compare taCasp3 + ChR2-EGFP versus taCasp3 + EGFP groups). These results demonstrated that heightened astrocyte $Ca^{2+}$ dynamics are necessary for the pBF cholinergic input–mediated modulation of fear extinction.

### Donepezil increases astrocyte $Ca^{2+}$ activity and facilitates fear extinction

Our results showed that the increases of cholinergic neurotransmission and of extracellular ACh during fear extinction enhanced astrocyte $Ca^{2+}$ activity in the CA1 region; this neuron-glia signaling pathway enhanced fear memory extinction. At present, the enhancement of the cholinergic neurotransmission represents a main approach in the treatment of cognitive and behavioral symptoms of mild and moderate stages of Alzheimer's disease (AD) (*43*); the main class of drugs currently used is acetylcholinesterase inhibitors, such as donepezil (*43*, *44*). Whether donepezil, the widely used memory and cognitive improvement drug, could enhance astrocyte $Ca^{2+}$ activity and facilitate fear extinction are feats worth testing. We recorded astrocyte $Ca^{2+}$ activity (using virally expressed GCaMP6f) after local injection of saline or donepezil (0.1 mM) in the CA1 region (Fig. 7A). Compared with saline injection, donepezil induced a significant increase of astrocytic $Ca^{2+}$ activity (Fig. 7, B and C).

To test the role of donepezil in fear extinction, saline or donepezil (0.1 mM) was bilaterally injected into CA1 regions before fear extinction on day 2 (Fig. 7D). These saline- or donepezil-treated mice had comparable learning curves for fear conditioning on day 1 (Fig. 7D). However, the donepezil injection group showed significantly facilitated fear extinction on day 2 and decreased fear memory on day 3 (Fig. 7D). Donepezil injection did not affect mice motor performance in the open-field test (fig. S14, A to C). Together, these results indicated that donepezil can facilitate fear extinction.

To further determine the therapeutic applicability of donepezil for fear extinction, we tested whether the IP injection of donepezil facilitates fear extinction. Mice were injected with saline or donepezil 30 min before the fear extinction training on day 2, and the extinction memory was assessed on day 3 (Fig. 7E). Saline or donepezil injection groups had comparable learning curves for fear conditioning on day1 (Fig. 7E). Donepezil (0.25 mg/kg, IP; allometry to human dose of 2.5 mg orally) had a facilitating effect on fear extinction on day 2 but did not affect the freezing level on day3 (Fig. 7E). A higher dose of donepezil (0.5 mg/kg, IP; allometry to human dose of 5 mg orally, which is the starting clinical dose for human) both significantly facilitated fear extinction on day 2 and decreased freezing level on day 3 (Fig. 7E). In addition, donepezil IP injection did not affect the motor performance in the open-field test (fig. S14, D to F). Therefore, pharmacological enhancement of the pBF cholinergic neuron to CA1 astrocyte pathway can facilitate fear extinction and holds promise in the treatment of fear- and anxiety-related disorders like PTSD.

## DISCUSSION

Fear extinction is an organismal internal defense mechanism against pathogenic fear when re-exposed to an environment that is no longer a threat or danger; this mechanism optimizes decision-making and allows better adaptation. Both animal and human studies have suggested that impaired fear extinction is critical in the development and maintenance of fear-related disorders, such as PTSD (*1*, *45*). Thus, revealing endogenous contributors to fear extinction is critical to deepen its understanding and to identify targets for improved treatments of fear-related disorders. Here, we discovered that de novo astrocytic $Ca^{2+}$ responses in the dCA1 region are critical for fear extinction; these responses were induced by increased pBF cholinergic input activity. Inhibition or activation of this pathway leads to impairment or facilitation in fear extinction, respectively. Targeting this pathway with the cholinesterase inhibitor donepezil elevated astrocyte $Ca^{2+}$ activity in the dCA1 region and facilitated fear extinction (Fig. 7F). Together, our findings add a key contribution to the field by unveiling the unacknowledged neuron-glia signaling pathway in control of fear extinction and suggest promising therapeutic interventions for fear-related disorders.

### CA1 astrocytes may serve as an important protector against excessive fear

Astrocyte physiological activity and function during fear extinction is scarcely explored. The *Fos* measurement in the current study revealed that the astrocytes in the CA1 region were significantly and specifically activated during fear extinction, while astrocytes in the amygdala and mPFC were activated during both extinction and non-extinction conditions. By using fiber photometry, we further found that the CA1 astrocytic $Ca^{2+}$ responsiveness was specifically primed by aversive experience and dependent on associated context. Astrocytic $Ca^{2+}$ signals were lower during fear retrieval than extinction training, and were inversely correlated with the freezing levels during fear extinction. This astrocytic responsiveness diminished when mice were relocated in a different neutral context and were absent during re-exposure in the NOR or reward-related context. On the contrary, a very recent study reported that elevated astrocyte $Ca^{2+}$ activity in the amygdala remains for days after conditioning, coupled with freezing bouts during recall, but not extinction sessions (*46*). Together, the specific responsiveness of CA1 astrocytes to extinction suggested a unique role that merited further investigation.

Our investigation further revealed that attenuating this CA1 astrocytic $Ca^{2+}$ activity impaired fear extinction. Conversely, increasing CA1 astrocytic $Ca^{2+}$ activity, specifically during the extinction training phase, enhanced fear extinction. These results suggest that the astrocytic responsiveness is both necessary and sufficient for governing natural fear extinction. Moreover, in our present study, the strength of astrocytic $Ca^{2+}$ responses diminished as the fear level drops after extinction, suggesting an adaptive role of CA1 astrocytes. Of note, our previous study found that the CA1 astrocyte activation post–fear memory acquisition disrupted memory consolidation and persistently decreased contextual fear memory (*19*). Together, we propose that CA1 astrocytes may serve an important endogenous protective entity against excessive fear by controlling natural fear extinction and can be of important biological significance for adaptation to previous traumatic events.

### pBF cholinergic signaling couples with CA1 astrocytic activity in control of fear extinction

Neuromodulation, including ACh signaling, shapes emotional learning in distributed neuronal circuits across the brain (*25*). The potential role of cholinergic neurons in traumatic stress–induced emotional memory regulation remains largely unexplored (*29*, *47*). By using a sensor to detect extracellular ACh levels, we observed de novo ACh signals preceding and coupling with astrocytic $Ca^{2+}$

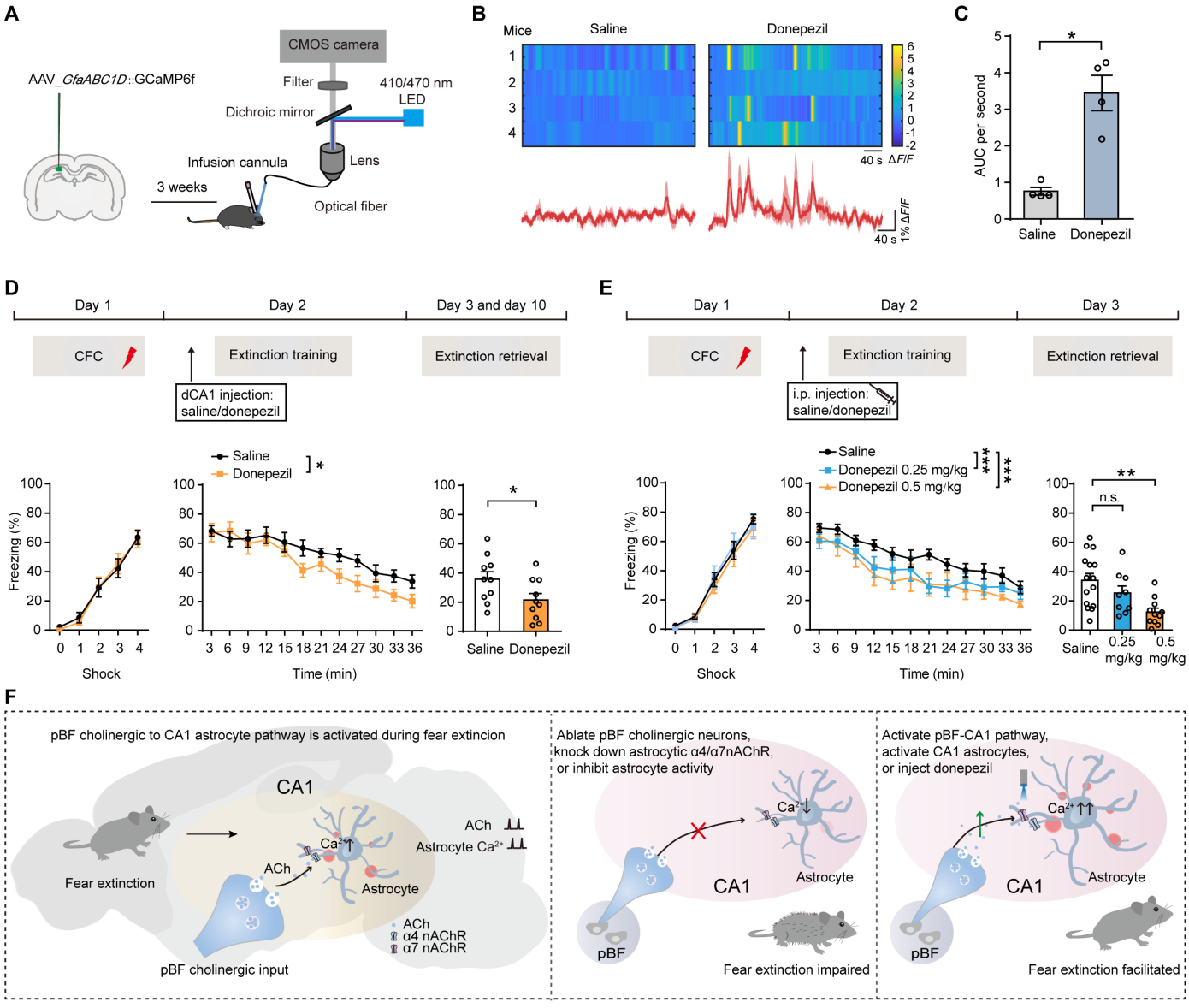


**Fig. 7. Acetylcholinesterase inhibitor donepezil increases astrocyte $Ca^{2+}$ activity and facilitates fear extinction.** (**A**) Diagram of viral microinjection and behavioral test. (**B**) Top and bottom: Heatmaps and averaged traces of Δ*F*/*F* astrocyte GCaMP6f signals in mice receiving saline or donepezil (1 μl) treatment ($n = 4$ per group). (**C**) Quantification of GCaMP6f AUC in saline- or donepezil-treated mice. (**D**) Intracranial microinjection of donepezil before extinction training–enhanced fear extinction training and decreased fear memory ($n = 10$ per group). (**E**) IP injection of donepezil before extinction training–enhanced fear extinction training and decreased fear memory ($n = 9$ to 11 per group). (**F**) Model summarizing the pBF cholinergic signaling to CA1 astrocytes in control fear extinction. ACh release in CA1 triggers astrocytic calcium activities through α4 and α7 subunits of nAChRs during fear extinction. Inhibition or activation of this cholinergic neurons to CA1 astrocyte signaling pathway leads to attenuation or facilitation in fear extinction, respectively. Error bars show means ± SEM. *$P < 0.05$, **$P < 0.01$, ***$P < 0.001$, as determined by paired *t* test (C), two-way ANOVA followed by Bonferroni's multiple comparisons test [(D) and (E), on day 2], and unpaired *t* test [(D) and (E), on day 3].

responses in the dCA1 region. The BF is the main cholinergic center that innervates the hippocampus (*47*, *48*). Our results showed that the cholinergic inputs from the BF to the dorsal hippocampal CA1 area originate mostly from the posterior part of the BF, as compared to its anterior. pBF cholinergic input activity was required and sufficient for the induction of CA1 astrocytic $Ca^{2+}$ responsiveness during fear extinction. Prolonged re-exposure into the fear conditioned context alone without "salient" stimuli such as a foot shock caused the activation of pBF cholinergic neurons due to the synaptic plasticity. It appears that the fear conditioning process made the formerly neutral context into a "salient" stimulus, possibly by affecting sensory gating (*49*). The afferents in pBF cholinergic neurons integrate the incoming sensory information of the fear conditioning–associated context, compare it with previous memory and send it to the cholinergic neurons, and activate it during fear extinction. Moreover, the pBF cholinergic input–induced astrocytic $Ca^{2+}$ responses in the dCA1 region were not dependent on the activity of the nearby neurons, but rather a consequence of "direct" pBF ACh

signaling to astrocytes. Perhaps this could be a spillover at the tripartite synapse whereby astrocytes surround pBF cholinergic terminals innervating pyramidal neurons and/or interneurons. A more crafty possibility could be if such pBF inputs would directly terminate on astrocytes forming synaptoids (*50*). Prior studies indicated that the cholinergic signaling could directly modulate hippocampal pyramidal neurons and enhance cognitive flexibility (*51*, *52*). However, the role of ACh signaling in hippocampal pyramidal cells during fear extinction remains to be determined.

Cholinergic neurons in the brain participate in essential functions via two major classes of receptors: mAChRs and nAChRs (*29*). α4 nAChR is permeable to calcium, and the level of $Ca^{2+}$ permeability is enough for significant increases in intracellular [$Ca^{2+}$] (*53*, *54*). α7 nAChR also has a relatively higher $Ca^{2+}$ permeability (*53*). We showed that the α4 and α7 subunits of astrocyte nAChRs, but not mAChRs, were responsible for the induction of astrocytic $Ca^{2+}$ responses. Electrophysiological study showed the cholinergic modulation of hippocampal pyramidal neurons through the muscarinic receptors but not nicotinic receptors (*51*, *52*). In addition, the α7 nAChR was reported to be important in mediating astrocytic responsiveness in the auditory cortex for cued fear memory persistence (*55*). Blocking α7 nAChR signaling in PFC attenuated trace fear extinction in adult but not juvenile rats possibly due to the late-adolescent maturation of the ventral hippocampal–PFC functional connectivity (*56*). These results combined with ours suggested possible segregation of cholinergic signaling and function in different cell types, brain regions, and life stages, which may allow intersection of targeted intervention.

Here, the evoked astrocytic $Ca^{2+}$ responses by cholinergic activation were significantly greater during fear extinction, which can be likely caused by the up-regulation of α4 and α7 subunit expression. This inference may be supported by previous findings that brief or prolonged nicotine or nicotinic receptor agonist treatments can cause the up-regulation of α4 or α7 subunit of nAChR expression (*57*, *58*). The prevalence of smoking (nicotine self-administration) among individuals with PTSD is particularly high (around 44.6%). Smokers with PTSD not only smoke more heavily compared to smokers without PTSD but also demonstrate greater nicotine dependence and lower quit rates following smoking cessation interventions (*59*). Smoking and nicotine dependence in PTSD suggests a mode of self-medication to activate the aforementioned nAChRs in the current study to allay fear.

We found that inhibiting astrocyte $Ca^{2+}$ activity or blocking astrocytic nAChR receptors abrogated the pro-extinction effect exerted by pBF cholinergic input activation. Moreover, ablation of pBF cholinergic neurons attenuated the astrocytic $Ca^{2+}$ responses and impaired fear extinction, while simultaneous activation of CA1 astrocytes rescued the deficits in extinction. These findings are different from the previous report that selective lesions of aBF, such as MS/DBB, and its cholinergic input to the dorsal or ventral hippocampus have no effect on fear extinction memory (*60*). Our findings offer an alternative scenario whereby dorsal hippocampus–projecting cholinergic neurons mainly locate in the pBF, suggesting that the pBF is critical for fear extinction. Furthermore, the above results indicate that pBF ACh signaling and astrocyte $Ca^{2+}$ activity are coupled so that cholinergic inputs to CA1 astrocytes govern fear extinction. Consistent with our discovery, clinical studies found that patients with traumatic brain injury have reduced gray matter density in the BF and hippocampus (*61*), which may explain frequent comorbidity of this injury with PTSD (*7*, *62*, *63*). Moreover, AD patients have degeneration of the basal forebrain cholinergic system (*64*) and they display deficits in fear extinction (*65*). We found that the cholinesterase inhibitor donepezil, at an allometry dose to the usual starting dose of 5 mg used in human therapy, enhanced astrocytic $Ca^{2+}$ response and facilitated fear extinction. Donepezil can have effect on both neurons and astrocytes (*66*, *67*). However, the dosage of drug is an important determinant of its final effect. On the basis of the previous studies that donepezil at low dosage had no effect on neuronal spontaneous activity and network oscillations (*66*, *68*), in the current study donepezil of the dosage used may have limited impact on CA1 neurons. Therefore, our findings demonstrate that the pBF cholinergic pathway to CA1 astrocytes plays a key role in fear extinction and provide promising therapeutic strategy for fear- and anxiety-related disorders.

## MATERIALS AND METHODS

### Animals

The ChAT-IRES-Cre knock-in mice were obtained from The Jackson Laboratory (RRID: IMSR_JAX:006410). C57BL/6J congenic mice were purchased from Shanghai SLAC Laboratory Animal Co. Ltd. All mice were housed with food and water available ad libitum in a temperature-controlled room with a 12-hour light/dark cycle (lights on at 07:00 a.m.). Mice were socially housed in numbers of two to five littermates until surgery. After surgery, mice were singly housed. Both female and male mice were used in all experiments. All mice groups were subjected to the same surgical and behavioral manipulations. All experimental procedures were in accordance with the guidelines of the International Association by the Zhejiang Chinese Medical University Animal Experimentation Committee (20210802-16). All surgeries were performed under sodium pentobarbital anesthesia, and every effort was made to minimize suffering.

### Stereotactic surgery

Mice were anesthetized with pentobarbital sodium (1%) and placed on a stereotaxic frame. Standard stereotactic procedures were performed as previously described (*19*). Body temperature was maintained throughout the procedure with a heating pad. Viruses were injected via a microsyringe, the needle of which was left in place for 10 to 15 min after the end of infusion to allow diffusion of the viruses. The positions of all injections were verified histologically after behavior experiments.

For activation of astrocytes and attenuation of astrocyte activity, 150 nl of each AAV2/5_*GfaABC1D*::ChR2-EGFP (Taitool Bioscience, diluted to $2.58 \times 10^{12}$ vg $ml^{-1}$), AAV2/5_*GfaABC1D*::hM3Dq-mCherry (Taitool Bioscience, diluted to $2.57 \times 10^{12}$ vg $ml^{-1}$), and AAV5_*GfaABC1D*::mCherry-hPMCA2w/b (Addgene plasmid #111568, diluted to $4.72 \times 10^{12}$ vg $ml^{-1}$) was bilaterally injected into the CA1 region [Anteroposterior (AP), −2.0 mm; Mediolateral (ML), ±1.4 mm; Dorsoventral (DV), −1.4 mm relative to bregma]. AAV2/5_*GfaABC1D*::EGFP and AAV2/5_*GfaABC1D*::mCherry were used as corresponding controls (Taitool Bioscience, diluted to $3.0 \times 10^{12}$ vg $ml^{-1}$ and $2.69 \times 10^{12}$ vg $ml^{-1}$). Three weeks following viral injection, an optical fiber was implanted into the CA1 region of each mouse (AP, −2.0 mm; ML, ±1.4 mm; DV, −1.2 mm relative to bregma).

For optogenetic activation of cholinergic neurons, 120 nl of each AAV2/9_*hEF1*α:: DIO-ChR2-EYFP (Taitool Bioscience, diluted to

$4.23 \times 10^{12}$ vg $ml^{-1}$) and AAV2/9_*hSyn*::FLEX-ChrimsonR-tdTomato (Taitool Bioscience, diluted to $6.33 \times 10^{12}$ vg $ml^{-1}$) was bilaterally injected into the pBF (AP, 0.2 mm; ML, ±1.2 mm; DV, −5.4 mm relative to bregma) in ChAT-IRES-Cre mice. AAV2/9_*hEF1*α::DIO-EYFP (Taitool Bioscience, diluted to $4.08 \times 10^{12}$ vg $ml^{-1}$) was used as corresponding control. Three weeks following viral injection, optical fibers were implanted into CA1 areas of mice.

For the ablation of cholinergic neurons, 120 nl of AAV2/9_*hEF1*α::FLEX-taCasp3-TEVp-WPRE-hGH-pA (BrainVTA, diluted to $5.23 \times 10^{12}$ vg $ml^{-1}$) was bilaterally injected into the pBF in ChAT-IRES-Cre mice.

For $Ca^{2+}$ imaging, AAV5_*GfaABC1D*::GCaMP6f (BrainVTA, diluted to $2.21 \times 10^{12}$ vg $ml^{-1}$) and AAV5_*GfaABC1D*::jRGECO1a (BrainVTA, diluted to $5.62 \times 10^{12}$ vg $ml^{-1}$) were unilaterally injected into the CA1 region, while AAV2/9_*hEF1*α::DIO axon-GCaMP6s (BrainVTA, diluted to $3.21 \times 10^{12}$ vg $ml^{-1}$) was unilaterally injected into the pBF. Three weeks following viral injection, an optical fiber was implanted into the CA1 region or pBF (AP, 0.2 mm; ML, ±1.2 mm; DV, −5.2 mm relative to bregma).

For neurotransmitter sensor imaging, AAV2/9_*hSyn*::5-HT3.0 (Brain Case, diluted to $5.0 \times 10^{12}$ vg $ml^{-1}$), AAV2/9_*GfaABC-1D*::gACh4h (provided from Y. Li Lab, Peking University, diluted to $3.16 \times 10^{12}$ vg $ml^{-1}$), AAV2/9_*hSyn*::rAChmut (BrainVTA, diluted to $2.51 \times 10^{12}$ vg $ml^{-1}$), or AAV2/5_*GfaABC1D*::cATP1.0 (Brain Case, diluted to $3.09 \times 10^{12}$ vg $ml^{-1}$) was unilaterally injected into the CA1 region. Three weeks following viral injection, an optical fiber was implanted into the CA1 region of each mouse for imaging.

To knock down the level of α4 or α7 nAChR in astrocytes in vivo, AAV2/5_*GfaABC1D*::RNAi(α4nAChR) (Taitool Bioscience, diluted to $6.3 \times 10^{12}$ vg $ml^{-1}$) or AAV2/5_*GfaABC1D*::RNAi(α7nAChR) (Taitool Bioscience, diluted to $7.0 \times 10^{12}$ vg $ml^{-1}$) were bilaterally injected into the CA1 region. AAV2/5_*GfaABC1D*::mCherry were used as corresponding controls.

For optogenetic fiber implantation, two optical fibers (core diameter, 200 mm; numerical aperture, 0.37) were bilaterally implanted into CA1 regions (AP, −2.0 mm; ML, ±1.4 mm; DV, −1.2 mm relative to bregma).

For pharmacological experiments, guide cannulae were bilaterally implanted into CA1 regions at the above coordinates for drug infusion at 100 nl/min using a microinfusion pump. Atropine (Sigma-Aldrich, A0257), MECA (Sigma-Aldrich, M9020), DHβE (Tocris Bioscience, 2349), MLA (Abcam, Ab120072), and donepezil HCl (Selleck, S2462) were dissolved and diluted to their final concentrations in sterile 0.9% NaCl saline.

For photostimulation coupled with pharmacological experiments, an optical fiber (AP, −2.0 mm; ML, +1.1 mm; DV, −1.5 mm relative to bregma, at a 10° angle) and an infusion cannula (AP, −2 mm; ML, +1.9 mm; DV, −0.7 mm relative to bregma, at a 20° angle) were unilaterally implanted into the CA1 region for simultaneous photostimulation and drug infusion.

### Contextual fear extinction behavior protocol

The fear extinction tasks were carried out in a 25 cm × 25 cm × 25 cm chamber (Panlab Harvard Apparatus) with grid floors placed inside a sound-protected box (original conditioning context). On day 1, the fear conditioning phase, mice were habituated in the conditioning chamber for 5 min, followed by four footshocks (US, 0.6 mA, 2 s) with an interval of 60 s. Mice remained in the conditioning chamber for a 90-s consolidation period following the last US and then returned to their home cages. The chamber was cleaned with rubbing alcohol. Twenty-four hours after fear conditioning, mice were returned to the fear conditioning chamber to receive 40-min extinction training without any US. Mice were then put back to their home cages for another 24 hours. On day 3, mice were placed in the conditioned context for 5-min extinction memory retrieval test. The data were automatically recorded using commercial software (FREEZING, Panlab Harvard Apparatus). Used as control, context B was different from the fear conditioning chamber before, was designed with white plastic floors and curved walls with visual cues, and cleaned with 1% acetic acid to be different from the original conditioning context.

### In vivo fiber photometry recording

We used a fiber photometry system (Thinker Tech) to record the fluorescence signals in freely moving mice. Purple (405 nm) light-emitting diode (LED) light was band-pass filtered (405/10 nm, model 65133, Edmund Optics), blue (473 nm) LED light (Cree LED) was band-pass filtered (470/25 nm, model 65144, Edmund Optics), and yellow (580 nm) LED light (Cree LED) was band-pass filtered (572/28 nm, model 84100, Edmund Optics). Light beam was reflected by a dichroic mirror (model 67079, 495-nm long pass, Edmund Optics) and passed through a multi-band fitter (model 87-282, Edmund Optics), before being focused using a 20× objective lens (Olympus) and funneled into an optical fiber, and the light was guided between the commutator and the implanted optical fiber cannula. The laser power at the tip of the optical fiber was adjusted to 40 μW (470 nm) and 60 μW (580 nm) to minimize photobleaching. The 405-nm signal (20 μW) was further used to correct movement artifacts. Finally, the emitted green (500 to 530 nm) and red (605 to 625 nm) fluorescent light was recorded using a scientific complementary metal-oxide semiconductor camera.

For contextual fear extinction behavior, mice underwent the 3-day contextual fear extinction procedure, as described above. During CFC on day 1, freezing behavior and $Ca^{2+}$ signals of subjects were recorded for 5-min habituation, then four footshocks were delivered with 60-s interval time. $Ca^{2+}$ signals were recorded during 40-min fear extinction training on day 2. The 0- to 5-min epoch was considered as the fear retrieval stage. The remaining epochs together were considered as the extinction training stage.

The fiber photometry coupled with the optogenetics system (Inper) was as follows. Briefly, the excitation light from blue (470 nm) and red (620 nm) light sources was merged into one beam through a dichroic mirror. The beam was funneled into a multimode fiber and then transmitted to the specified brain region to excite the GFP (such as GCaMP6) and corresponding red channelrhodopsin (such as ChrimsonR). The emitted green light was collected by a multimode fiber and transformed into an electrical signal by weak signal detector. Heatmaps and averaged $Ca^{2+}$ traces were plotted using a self-developed MATLAB program.

To report average fluorescence signal within a session, $\Delta F/F$ was calculated as $(F - F_0)/F_0$ and $F_0$ is the mean value of the prestimulus signal for each trial. To analyze the correlation and time course relationship of the astrocyte $Ca^{2+}$ and ACh signals, we defined the signal onset as the time when the signal increased above 10% of its peak amplitude in the rising edge. The time to peak is the time from onset to peak of a signal. We defined the rise time as the time

required for the rising edge of the signal to go from 10% to 90% of its peak amplitude according to previous study (*69*).

### Optogenetic manipulation

For optogenetic stimulation during fear extinction on day 2, following the recording of the baseline freezing levels during the first 3 min, we initiated the light stimulation at the third minute with 11 consecutive 3-min epochs consisting of 1-min light on, 1-min light off, and 1-min light on periods (473 nm, 1 to 3 mW at the fiber tip).

For optogenetic stimulation during fear retrieval on day 3, we initiated the light stimulation at the first minute of fear retrieval and lasted 5 min with 1-min light on and 1-min light off (473 nm, 1 to 3 mW at the fiber tip). For optogenetic stimulation during the open-field test, we used a 3-min epoch as the paradigm consisting of 1-min light off, 1-min light on, and 1-min light off.

### Chemogenetic manipulation

For chemogenetic manipulation, CNO (Abcam, catalog no. Ab14-1704; dissolved in 0.9% NaCl saline), at the dose of 1 mg/kg body weight, was injected intraperitoneally into mice expressing hM3Dq-mCherry (Fig. 3 and fig. S3). Behavioral tests started 30 min after injection. For local chemogenetic manipulation (fig. S6), CNO (10 μM, 200 nl, dissolved in artificial cerebrospinal fluid) was infused into the dCA1 region through cannulae, at 50 nl/min using a microinfusion pump.

### Open-field test

Mice were placed in the corner of the square open-field arena (40 cm × 40 cm × 40 cm) at the start of the experiment and allowed to freely explore for 5 min. The center of the open field was defined as the central 50% of the arena. The locomotor activity of the mice was video-recorded and analyzed with automatic behavioral tracking software (ANY-maze, Stoelting Co., USA).

### Novel object recognition

According to previous study (*19*), mice were habituated to investigator handling for 5 min and habituated to a square testing arena (40 cm × 40 cm × 40 cm) for 10 min per day on three consecutive days. After habituation, the NOR task was divided into a sample phase and a test phase, each lasting 5 min. In the sample phase, mice were placed in the arena, exposed to two identical objects (A and B), and then returned to its home cage. Twenty-four hours after the sample phase, mice were returned to the arena for the test phase when exposed to two objects, one was the same as in the sample phase (A) and the other one was replaced with a novel object (C). The time spent in exploring each object was recorded. Exploration was defined as touching the object with the nose or directing the nose to the object at a distance of no more than 2 cm.

### Sucrose reward experiment

Mice were given access to a bottle containing 5% sucrose aqueous solution in the observation cage on day 1. Mice were put in the same cage to explore for 10 min without sucrose on day 2. $Ca^{2+}$ and neurotransmitter sensor signals were recorded on days 1 and 2.

### Histology

After experiments, the positions of the optical fibers and cannulae were verified histologically. Mice with incorrect positioning of optical fibers or cannulae were excluded from analysis.

#### *Immunohistological staining*

Mice were anesthetized with sodium pentobarbital and then perfused transcardially with phosphate-buffered saline (PBS) followed by 4% paraformaldehyde in PBS (PFA; w/v). Brains were postfixed in 4% PFA in PBS at 4°C overnight and then cryoprotected in 30% aqueous solution of sucrose (w/v) for 2 to 3 days at 4°C. Coronal sections (40 μm) were cut on a microtome (Thermo Fisher Scientific) and stored in PBS at 4°C for further use. For immunostaining, each section was permeabilized with 0.5% Triton X-100 in PBS (v/v) for 10 min. After washing with PBS, the nonspecific binding of sections was blocked in PBS containing 10% bovine serum albumin (BSA; w/v) and 5% donkey serum (v/v) at room temperature (20° to 25°C) for 1 hour and then incubated with the primary antibody in PBS at 4°C for 24 hours. The sections were then washed three times in PBS for 10 min, followed by incubation with the secondary antibody at room temperature for 2 hours. Primary antibodies used were rabbit anti-GFAP (Millipore, AB5804, 1:1000), mouse anti-NeuN (Millipore, MAB377, 1:500), mouse anti-S100β (Sigma-Aldrich, S2532, 1:500), rabbit anti-DsRed (Clontech, 632496, 1:500), mouse anti–c-*Fos* (Proteintech, 66590-1-Ig, 1:1000), and goat anti-ChAT antibody (Millipore, AB144P, 1:500). Secondary antibodies used were donkey anti-rabbit Alexa Fluor 594 (Abcam, ab150076, 1:1000), donkey anti-mouse Alexa Fluor 647 (Abcam, ab150107, 1:1000), donkey anti-rabbit Alexa Fluor 488 (Abcam, ab150073, 1:1000), and donkey anti-mouse Alexa Fluor 488 (Abcam, ab150105, 1:1000). Slides were washed three times with PBS for 10 min. Finally, the sections were mounted on microscope slides and covered by a glass coverslip (*19*). Fluorescence images were acquired with an Olympus FV-3000 (Japan) confocal microscope. For $Fos^{+}$ cell quantification, all brain sections containing the brain areas of interest were obtained from mouse brains. Every fourth brain sections were collected and stained with c-*Fos* antibody, and the mean value for each mouse was then calculated.

#### *RNAscope in situ hybridization*

To examine transcripts of *Chrna4* and *Chrna7* genes encoding α4 and α7 subunits of nAChR, respectively, we performed in situ hybridization using the RNAscope Multiplex Fluorescent Reagent Kit v2 [Advanced Cell Diagnostics (ACD), 323100] according to the manufacturer's instructions. Sections were pretreated with hydrogen peroxide, target retrieval reagents, and protease digestion and then were hybridized with prewarmed *Chrna4* mRNA probe (ACD, 429871), *Chrna7* mRNA probe (ACD, 465161-C2), positive control probe (ACD, 320881), or negative control probe (ACD, 320871), followed by amplifier1, amplifier2, and amplifier3 successively for 15 to 30 min. For *Chrna4* mRNA, the sections were further incubated in horseradish peroxidase–channel 1 (HRP-C1) for 15 min and TSA Vivid 520 (PG-323271) or 650 (PG-323273) for 30 min to fluorescently label probes. An HRP blocker was added for 15 min. Then, for *Chrna7* mRNA, the sections were incubated in HRP-C2 for 15 min and TSA Vivid 520 or 650 for 30 min to fluorescently label probes. Finally, an HRP blocker was added for 15 min. All hybridization and incubation steps were performed at 40°C in the hybridization oven. GFAP immunohistochemical staining was obtained upon completion of the in situ hybridization protocol.

### $Ca^{2+}$ imaging

Following procedures described in previous study (*19*). $Ca^{2+}$ imaging in hippocampal slices (300 μm) was made from 8-week-old mice.

Slices were then incubated for 1 hour in a holding chamber with oxygenated normal $Ca^{2+}$ artificial cerebrospinal fluid at 35°C and then kept at 32°C. Individual slices were transferred to a submerged recording chamber. For recording light stimulation–induced $Ca^{2+}$ signals, astrocytes were bulk loaded in slices with Rhod-2 AM (20 μM, Invitrogen). The fluorescence intensity was measured at an excitation wavelength of 550 nm and emission wavelength of 580 nm. $Ca^{2+}$ signals were calculated as the relative change in fluorescence ($\Delta F/F$), where $F$ is the fluorescence intensity before photostimulation and $\Delta F$ is the change in fluorescence after photostimulation.

### Statistical analyses

Sample sizes and statistical tests can be found in the figure legends. GraphPad Prism (version 10.1.2) and MATLAB (MathWorks) were used for statistical analysis. The sample size required for an individual set of experiments was pre-assessed using power analysis (set at 80% and $\alpha = 0.05$), and the normality of data was established using D'Agostino-Pearson or Shapiro-Wilk tests for normality. We used one-way or two-way analysis of variance (ANOVA) followed by the Bonferroni or Dunn's post hoc tests, and standard two-tailed paired or unpaired $t$ tests. Animals were randomly assigned to treatment groups. Both the researchers conducting the experiments and those analyzing the data will be blinded to the group assignments. Data are presented as means ± SEM. Statistical significance was set at $P < 0.05$.

## Supplementary Materials

**This PDF file includes:**

Figs. S1 to S14

## REFERENCES AND NOTES


1. K. J. Ressler, Translating across circuits and genetics toward progress in fear- and anxiety-related disorders. *Am. J. Psychiatry* **177**, 214–222 (2020).
2. R. K. Pitman, A. M. Rasmusson, K. C. Koenen, L. M. Shin, S. P. Orr, M. W. Gilbertson, M. R. Milad, I. Liberzon, Biological studies of post-traumatic stress disorder. *Nat. Rev. Neurosci.* **13**, 769–787 (2012).
3. M. G. Craske, C. F. Sandman, M. B. Stein, How can neurobiology of fear extinction inform treatment? *Neurosci. Biobehav. Rev.* **143**, 104923 (2022).
4. K. A. Knowles, D. F. Tolin, Mechanisms of action in exposure therapy. *Curr. Psychiatry Rep.* **24**, 861–869 (2022).
5. B. Vervliet, M. G. Craske, D. Hermans, Fear extinction and relapse: State of the art. *Annu. Rev. Clin. Psychol.* **9**, 215–248 (2013).
6. K. M. Myers, M. Davis, Mechanisms of fear extinction. *Mol. Psychiatry* **12**, 120–150 (2007).
7. K. J. Ressler, S. Berretta, V. Y. Bolshakov, I. M. Rosso, E. G. Meloni, S. L. Rauch, W. A. Carlezon Jr., Post-traumatic stress disorder: Clinical and translational neuroscience from cells to circuits. *Nat. Rev. Neurol.* **18**, 273–288 (2022).
8. S. Maren, A. Holmes, Stress and fear extinction. *Neuropsychopharmacology* **41**, 58–79 (2016).
9. C. A. Orsini, S. Maren, Neural and cellular mechanisms of fear and extinction memory formation. *Neurosci. Biobehav. Rev.* **36**, 1773–1802 (2012).
10. D. I. Choi, J. Kim, H. Lee, J.-I. Kim, Y. Sung, J. E. Choi, S. Jayakumar Venkat, P. Park, H. Jung, B.-K. Kaang, Synaptic correlates of associative fear memory in the lateral amygdala. *Neuron* **109**, 2717–2726.e3 (2021).
11. F. H. Do-Monte, G. Manzano-Nieves, K. Quinones-Laracuente, L. Ramos-Medina, G. J. Quirk, Revisiting the role of infralimbic cortex in fear extinction with optogenetics. *J. Neurosci.* **35**, 3607–3615 (2015).
12. E. Baldi, C. Bucherelli, Brain sites Involved in fear memory reconsolidation and extinction of rodents. *Neurosci. Biobehav. Rev.* **53**, 160–190 (2015).
13. N. Whittle, J. Fadok, K. P. MacPherson, R. Nguyen, P. Botta, S. B. E. Wolff, C. Muller, C. Herry, P. Tovote, A. Holmes, N. Singewald, A. Luthi, S. Ciocchi, Central amygdala micro-circuits mediate fear extinction. *Nat. Commun.* **12**, 4156 (2021).
14. M. Bocchio, S. Nabavi, M. Capogna, Synaptic plasticity, engrams, and network oscillations in amygdala circuits for storage and retrieval of emotional memories. *Neuron* **94**, 731–743 (2017).
15. T. Amano, C. T. Unal, D. Pare, Synaptic correlates of fear extinction in the amygdala. *Nat. Neurosci.* **13**, 489–494 (2010).
16. A. F. Lacagnina, E. T. Brockway, C. R. Crovetti, F. Shue, M. J. McCarty, K. P. Sattler, S. C. Lim, S. L. Santos, C. A. Denny, M. R. Drew, Distinct hippocampal engrams control extinction and relapse of fear memory. *Nat. Neurosci.* **22**, 753–761 (2019).
17. A. Araque, V. Parpura, R. P. Sanzgiri, P. G. Haydon, Tripartite synapses: Glia, the unacknowledged partner. *Trends Neurosci.* **22**, 208–215 (1999).
18. Z. Tan, Y. Liu, W. Xi, H. F. Lou, L. Zhu, Z. Guo, L. Mei, S. Duan, Glia-derived ATP inversely regulates excitability of pyramidal and CCK-positive neurons. *Nat. Commun.* **8**, 13772 (2017).
19. Y. Li, L. Li, J. Wu, Z. Zhu, X. Feng, L. Qin, Y. Zhu, L. Sun, Y. Liu, Z. Qiu, S. Duan, Y.-Q. Yu, Activation of astrocytes in hippocampus decreases fear memory through adenosine $A_1$ receptors. *eLife* **9**, e57155 (2020).
20. S. Tewari, V. Parpura, A possible role of astrocytes in contextual memory retrieval: An analysis obtained using a quantitative framework. *Front. Comput. Neurosci.* **7**, 145 (2013).
21. J. Nagai, X. Z. Yu, T. Papouin, E. J. Cheong, M. R. Freeman, K. R. Monk, M. H. Hastings, P. G. Haydon, D. Rowitch, S. Shaham, B. S. Khakh, Behaviorally consequential astrocytic regulation of neural circuits. *Neuron* **109**, 576–596 (2021).
22. A. Adamsky, A. Kol, T. Kreisel, A. Doron, N. Ozeri-Engelhard, T. Melcer, R. Refaeli, H. Horn, L. Regev, M. Groysman, M. London, I. Goshen, Astrocytic activation generates de novo neuronal potentiation and memory enhancement. *Cell* **174**, 59–71.e14 (2018).
23. M. Martin-Fernandez, S. Jamison, L. M. Robin, Z. Zhao, E. D. Martin, J. Aguilar, M. A. Benneyworth, G. Marsicano, A. Araque, Synapse-specific astrocyte gating of amygdala-related behavior. *Nat. Neurosci.* **20**, 1540–1548 (2017).
24. X. C. Fan, C. N. Ma, J. C. Song, Z. H. Liao, N. Huang, X. Liu, L. Ma, Rac1 signaling in amygdala astrocytes regulates fear memory acquisition and retrieval. *Neurosci. Bull.* **37**, 947–958 (2021).
25. E. Likhtik, J. P. Johansen, Neuromodulation in circuits of aversive emotional learning. *Nat. Neurosci.* **22**, 1586–1597 (2019).
26. H. Hirase, Y. Iwai, N. Takata, Y. Shinohara, T. Mishima, Volume transmission signalling via astrocytes. *Philos. Trans. R. Soc. Lond. B Biol. Sci.* **369**, 20130604 (2014).
27. K. V. Kastanenka, R. Moreno-Bote, M. De Pittá, G. Perea, A. Eraso-Pichot, R. Masgrau, K. E. Poskanzer, E. Galea, A roadmap to integrate astrocytes into systems neuroscience. *Glia* **68**, 5–26 (2020).
28. M. E. Hasselmo, J. M. Bower, Acetylcholine and memory. *Trends Neurosci.* **16**, 218–222 (1993).
29. M. R. Ananth, P. Rajebhosale, R. Kim, D. A. Talmage, L. W. Role, Basal forebrain cholinergic signalling: Development, connectivity and roles in cognition. *Nat. Rev. Neurosci.* **24**, 233–251 (2023).
30. X. Yu, A. M. W. Taylor, J. Nagai, P. Golshani, C. J. Evans, G. Coppola, B. S. Khakh, Reducing astrocyte calcium signaling in vivo alters striatal microcircuits and causes repetitive behavior. *Neuron* **99**, 1170–1187.e9 (2018).
31. X. Yu, J. Nagai, B. S. Khakh, Improved tools to study astrocytes. *Nat. Rev. Neurosci.* **21**, 121–138 (2020).
32. J. Chen, Z. Tan, L. Zeng, X. Zhang, Y. He, W. Gao, X. Wu, Y. Li, B. Bu, W. Wang, S. Duan, Heterosynaptic long-term depression mediated by ATP released from astrocytes. *Glia* **61**, 178–191 (2013).
33. K. Noh, W. H. Cho, B. H. Lee, D. W. Kim, Y. S. Kim, K. Park, M. Hwang, E. Barcelon, Y. K. Cho, C. J. Lee, B. E. Yoon, S. Y. Choi, H. Y. Park, S. B. Jun, S. J. Lee, Cortical astrocytes modulate dominance behavior in male mice by regulating synaptic excitatory and inhibitory balance. *Nat. Neurosci.* **26**, 1541 (2023).
34. Y. Mu, D. V. Bennett, M. Rubinov, S. Narayan, C. T. Yang, M. Tanimoto, B. D. Mensh, L. L. Looger, M. B. Ahrens, Glia accumulate evidence that actions are futile and suppress unsuccessful behavior. *Cell* **178**, 27 (2019).
35. H. Chai, B. Diaz-Castro, E. Shigetomi, E. Monte, J. C. Octeau, X. Yu, W. Cohn, P. S. Rajendran, T. M. Vondriska, J. P. Whitelegge, G. Coppola, B. S. Khakh, Neural circuit-specialized astrocytes: Transcriptomic, proteomic, morphological, and functional evidence. *Neuron* **95**, 531–549.e9 (2017).
36. N. Bazargani, D. Attwell, Astrocyte calcium signaling: The third wave. *Nat. Neurosci.* **19**, 182–189 (2016).
37. F. Deng, J. Wan, G. Li, H. Dong, X. Xia, Y. Wang, X. Li, C. Zhuang, Y. Zheng, L. Liu, Y. Yan, J. Feng, Y. Zhao, H. Xie, Y. Li, Improved green and red GRAB sensors for monitoring spatiotemporal serotonin release in vivo. *Nat. Methods* **21**, 692–702 (2024).
38. H. Dannenberg, M. Pabst, O. Braganza, S. Schoch, J. Niediek, M. Bayraktar, F. Mormann, H. Beck, Synergy of direct and indirect cholinergic septo-hippocampal pathways coordinates firing in hippocampal networks. *J. Neurosci.* **35**, 8394–8410 (2015).
39. E. D. Melonakos, J. A. White, F. R. Fernandez, Gain modulation of cholinergic neurons in the medial septum-diagonal band of Broca through hyperpolarization. *Hippocampus* **26**, 1525–1541 (2016).
40. S. R. Cobb, C. H. Davies, Cholinergic modulation of hippocampal cells and circuits. *J. Physiol.* **562**, 81–88 (2005).
41. D. Knox, S. M. Keller, Cholinergic neuronal lesions in the medial septum and vertical limb of the diagonal bands of Broca induce contextual fear memory generalization and impair acquisition of fear extinction. *Hippocampus* **26**, 718–726 (2016).

42. L. Jiang, S. Kundu, J. D. Lederman, G. Y. López-Hernández, E. C. Ballinger, S. Wang, D. A. Talmage, L. W. Role, Cholinergic signaling controls conditioned fear behaviors and enhances plasticity of cortical-amygdala circuits. *Neuron* **90**, 1057–1070 (2016).
43. G. Marucci, M. Buccioni, D. D. Ben, C. Lambertucci, R. Volpini, F. Amenta, Efficacy of acetylcholinesterase inhibitors in Alzheimer's disease. *Neuropharmacology* **190**, 108352 (2021).
44. N. Zhang, M. L. Gordon, Clinical efficacy and safety of donepezil in the treatment of Alzheimer's disease in Chinese patients. *Clin. Interv. Aging* **13**, 1963–1970 (2018).
45. D. V. Zuj, M. A. Palmer, M. J. Lommen, K. L. Felmingham, The centrality of fear extinction in linking risk factors to PTSD: A narrative review. *Neurosci. Biobehav. Rev.* **69**, 15–35 (2016).
46. R. L. Suthard, R. A. Senne, M. D. Buzharsky, A. Y. Pyo, K. E. Dorst, A. H. Diep, R. H. Cole, S. Ramirez, Basolateral amygdala astrocytes are engaged by the acquisition and expression of a contextual fear memory. *J. Neurosci.* **43**, 4997–5013 (2023).
47. D. Knox, V. Parikh, Basal forebrain cholinergic systems as circuits through which traumatic stress disrupts emotional memory regulation. *Neurosci. Biobehav. Rev.* **159**, 105569 (2024).
48. M. M. Mesulam, E. J. Mufson, A. I. Levey, B. H. Wainer, Cholinergic innervation of cortex by the basal forebrain: Cytochemistry and cortical connections of the septal area, diagonal band nuclei, nucleus basalis (substantia innominata), and hypothalamus in the rhesus monkey. *J. Comp. Neurol.* **214**, 170–197 (1983).
49. M. J. Nobre, A. Cabral, M. L. Brandão, GABAergic regulation of auditory sensory gating in low- and high-anxiety rats submitted to a fear conditioning procedure. *Neuroscience* **171**, 1152–1163 (2010).
50. A. Verkhratsky, V. Parpura, Recent advances in (patho)physiology of astroglia. *Acta Pharmacol. Sin.* **31**, 1044–1054 (2010).
51. X. W. Li, Y. Ren, D. Q. Shi, L. Qi, F. Xu, Y. Y. Xiao, P. M. Lau, G. Q. Bi, Biphasic cholinergic modulation of reverberatory activity in neuronal networks. *Neurosci. Bull.* **39**, 731–744 (2023).
52. J. Palacios-Filardo, M. Udakis, G. A. Brown, B. G. Tehan, M. S. Congreve, P. J. Nathan, A. J. H. Brown, J. R. Mellor, Acetylcholine prioritises direct synaptic inputs from entorhinal cortex to CA1 by differential modulation of feedforward inhibitory circuits. *Nat. Commun.* **12**, 5475 (2021).
53. D. S. McGehee, L. W. Role, Physiological diversity of nicotinic acetylcholine receptors expressed by vertebrate neurons. *Annu. Rev. Physiol.* **57**, 521–546 (1995).
54. A. P. Haghighi, E. Cooper, A molecular link between inward rectification and calcium permeability of neuronal nicotinic acetylcholine alpha3beta4 and alpha4beta2 receptors. *J. Neurosci.* **20**, 529–541 (2000).
55. K. Zhang, R. Förster, W. He, X. Liao, J. Li, C. Yang, H. Qin, M. Wang, R. Ding, R. Li, T. Jian, Y. Wang, J. Zhang, Z. Yang, W. Jin, Y. Zhang, S. Qin, Y. Lu, T. Chen, J. Stobart, B. Weber, H. Adelsberger, A. Konnerth, X. Chen, Fear learning induces α7-nicotinic acetylcholine receptor-mediated astrocytic responsiveness that is required for memory persistence. *Nat. Neurosci.* **24**, 1686–1698 (2021).
56. A. M. M. Miguelez Fernández, H. M. Molla, D. R. Thomases, K. Y. Tseng, Prefrontal α7nAChR signaling differentially modulates afferent drive and trace fear conditioning behavior in adolescent and adult rats. *J. Neurosci.* **41**, 1908–1916 (2021).
57. R. R. Jonnala, J. J. Buccafusco, Relationship between the increased cell surface alpha7 nicotinic receptor expression and neuroprotection induced by several nicotinic receptor agonists. *J. Neurosci. Res.* **66**, 565–572 (2001).
58. M. Alkondon, E. X. Albuquerque, Nicotinic receptor subtypes in rat hippocampal slices are differentially sensitive to desensitization and early in vivo functional up-regulation by nicotine and to block by bupropion. *J. Pharmacol. Exp. Ther.* **313**, 740–750 (2005).
59. E. B. Foa, A. Asnaani, D. Rosenfield, L. J. Zandberg, P. Gariti, P. Imms, Concurrent varenicline and prolonged exposure for patients with nicotine dependence and PTSD: A randomized controlled trial. *J. Consult. Clin. Psychol.* **85**, 862–872 (2017).
60. J. M. Staib, R. Della Valle, D. K. Knox, Disruption of medial septum and diagonal bands of Broca cholinergic projections to the ventral hippocampus disrupt auditory fear memory. *Neurobiol. Learn. Mem.* **152**, 71–79 (2018).
61. C. H. Salmond, D. A. Chatfield, D. K. Menon, J. D. Pickard, B. J. Sahakian, Cognitive sequelae of head injury: Involvement of basal forebrain and associated structures. *Brain* **128**, 189–200 (2005).
62. M. B. Stein, S. Jain, J. T. Giacino, H. Levin, S. Dikmen, L. D. Nelson, M. J. Vassar, D. O. Okonkwo, R. Diaz-Arrastia, C. S. Robertson, P. Mukherjee, M. McCrea, C. L. Mac Donald, J. K. Yue, E. Yuh, X. Sun, L. Campbell-Sills, N. Temkin, G. T. Manley, TRACK-TBI Investigators, O. Adeoye, N. Badjatia, K. Boase, Y. Bodien, M. R. Bullock, R. Chesnut, J. D. Corrigan, K. Crawford, R. Diaz-Arrastia, S. Dikmen, A.-C. Duhaime, R. Ellenbogen, V. R. Feeser, A. Ferguson, B. Foreman, R. Gardner, E. Gaudette, J. T. Giacino, L. Gonzalez, S. Gopinath, R. Gullapalli, J. C. Hemphill, G. Hotz, S. Jain, F. Korley, J. Kramer, N. Kreitzer, H. Levin, C. Lindsell, J. Machamer, C. Madden, A. Martin, T. McAllister, M. McCrea, R. Merchant, P. Mukherjee, L. D. Nelson, F. Noel, D. O. Okonkwo, E. Palacios, D. Perl, A. Puccio, M. Rabinowitz, C. S. Robertson, J. Rosand, A. Sander, G. Satris, D. Schnyer, S. Seabury, M. Sherer, M. B. Stein, S. Taylor, A. Toga, N. Temkin, A. Valadka, M. J. Vassar, P. Vespa, K. Wang, J. K. Yue, E. Yuh, R. Zafonte, Risk of posttraumatic stress disorder and major depression in civilian patients after mild traumatic brain injury: A TRACK-TBI study. *JAMA Psychiatry* **76**, 249–258 (2019).
63. A. C. McKee, M. E. Robinson, Military-related traumatic brain injury and neurodegeneration. *Alzheimers Dement.* **10**, S242–S253 (2014).
64. H. Hampel, M. M. Mesulam, A. C. Cuello, M. R. Farlow, E. Giacobini, G. T. Grossberg, A. S. Khachaturian, A. Vergallo, E. Cavedo, P. J. Snyder, Z. S. Khachaturian, The cholinergic system in the pathophysiology and treatment of Alzheimer's disease. *Brain* **141**, 1917–1933 (2018).
65. S. Nasrouei, J. A. Rattel, M. Liedlgruber, J. Marksteiner, F. H. Wilhelm, Fear acquisition and extinction deficits in amnestic mild cognitive impairment and early Alzheimer's disease. *Neurobiol. Aging* **87**, 26–34 (2020).
66. K. Skovgård, C. Agerskov, K. A. Kohlmeier, K. F. Herrik, The 5-HT receptor antagonist ondansetron potentiates the effects of the acetylcholinesterase inhibitor donepezil on neuronal network oscillations in the rat dorsal hippocampus. *Neuropharmacology* **143**, 130–142 (2018).
67. F. Alcantara-Gonzalez, I. Juarez, O. Solis, I. Martinez-Tellez, I. Camacho-Abrego, E. Masliah, R. Mena, G. Flores, Enhanced dendritic spine number of neurons of the prefrontal cortex, hippocampus, and nucleus accumbens in old rats after chronic donepezil administration. *Synapse* **64**, 786–793 (2010).
68. A. Eskandary, A. A. Moazedi, H. N. Zade, M. R. Akhond, Effects of donepezil hydrochloride on neuronal response of pyramidal neurons of the CA1 hippocampus in rat model of Alzheimer's disease. *Basic Clin. Neurosci.* **10**, 109–117 (2019).
69. W. Peng, Z. Wu, K. Song, S. Zhang, Y. Li, M. Xu, Regulation of sleep homeostasis mediator adenosine by basal forebrain glutamatergic neurons. *Science* **369**, eabb0556 (2020).


**Acknowledgments:** We are grateful to Y. Li from Peking University for providing the ACh sensor. We appreciate the great help/technical support/experimental support from the Medical Research Ctenter, Academy of Chinese Medical Sciences, Zhejiang Chinese Medical University. **Funding:** This work was supported by the National Key R&D Program of China (2021ZD0202803 to Z.C.), the National Natural Science Foundation of China (U23A20533 to Yi Wang, 32300851 to Y.L., and 82201564 to Lixuan Li), and Zhejiang Provincial Natural Science Foundation (LQ24H310008 to Y.L.). The funding sources were not involved in study design, data collection and interpretation, or in the decision to submit this research for publication.
**Author contributions:** Conceptualization: Y.L., Lixuan Li, Yi Wang, and Z.C. Methodology: Y.L., Lixuan Li, and Yibei Wang. Investigation: Y.L., Lixuan Li, Yibei Wang, X.L., X.D., Lingjie Li, and F.F. Visualization: Y.L., Lixuan Li, and Yibei Wang. Data curation: Y.L., Lixuan Li, Yi Wang, and X.L. Formal analysis: Y.L. Funding acquisition: Y.L., Lixuan Li, Yi Wang, and Z.C. Supervision: Yi Wang and Z.C. Writing—original draft: Y.L. and Lixuan Li Writing—review and editing: Y.L., Lixuan Li, Yibei Wang, Y.Z., L.C., S.D., V.P., Yi Wang, and Z.C. **Competing interests:** The authors declare that they have no competing interests. **Data and materials availability:** All data needed to evaluate the conclusions in the paper are present in the paper and/or the Supplementary Materials.

Submitted 26 August 2024
Accepted 28 February 2025
Published 4 April 2025
10.1126/sciadv.ads7191